Quaternary Science Reviews 357 (2025) 109323

Contents lists available at ScienceDirect

Quaternary Science Reviews

journal homepage: www.elsevier.com/locate/quascirev

Holocene hydroclimate and landscape changes as drivers of organic carbon cycling in a small northern Fennoscandian lake

Lilia E. Orozco[a,*], Jan Weckström[a,b], Mateusz Plociennik[c], Annika K. Åberg[d,e], J. Sakari Salonen[d], Darren R. Gröcke[f], Laura Arppe[g], Maijja Heikkilä[a,b,e]

[a] Ecosystems and Environment Research Programme, Faculty of Biological and Environmental Sciences, University of Helsinki, 00014, Finland
[b] Faculty of Biological and Environmental Sciences and Helsinki Institute of Sustainability Science (HELSUS), University of Helsinki, 00014, Finland
[c] Department of Invertebrate Zoology and Hydrobiology, University of Lodz, Lodz, Poland
[d] Department of Geosciences and Geography, University of Helsinki, 00014, Finland
[e] Geological Survey of Finland, Espoo, 02151, Finland
[f] Department of Earth Sciences, Durham University, Durham, United Kingdom
[g] Finnish Museum of Natural History LUOMUS, University of Helsinki, Helsinki, 00014, Finland

ARTICLE INFO

Handling Editor: A. Voelker

Keywords:
Arctic
Carbon burial
Carbon sources
Chironomids
Oxygen isotopes
Bayesian
Holocene

ABSTRACT

Lakes and ponds play a critical role in the high-latitude carbon cycle. Rapid climate warming, cryosphere degradation and increasing rainfall are transforming catchments and land-water interactions, altering lake carbon cycling in unprecedented ways. Here, we present Holocene (past 10.5 ka) sediment records from a small northern Fennoscandian lake to elucidate linkages of past hydroclimate change and lake carbon cycling. Using elemental and stable isotope composition of organic matter (C%, N%, δ^{13}C, δ^{15}N), age control from 23 radiocarbon dates, and a ground-penetrating radar survey of lake sediment layers, we reconstructed organic matter burial and sources, aided with a Bayesian end-member mixing model based on measurements from modern terrestrial and aquatic vegetation and particulate organic matter. The hydroclimate and lake hydrological regime changes were interpreted from lake-water δ^{18}O ($\delta^{18}O_{lw}$) reconstructed from subfossil chironomid (Chironomidae; non-biting midges) head capsules and δ^{18}O and δ^{2}H monitoring of local meteoric, lake and groundwaters. The $\delta^{18}O_{lw}$ and carbon burial mirror the Holocene temperature pattern, increasing in the cooler early Holocene, at their maxima in the warm mid-Holocene, and decreasing during the late Holocene cooling. The lake was dominated by aquatic organic matter through the Holocene, with benthic sources more dominant in the early Holocene and planktic in the late Holocene. A slight increase in the terrestrial organic matter proportion occurred in the warm and dry mid-Holocene despite reduced hydrological connectivity, which is contrary to the hypothesis that wetter climate increases allochtonous C burial. The higher mid-Holocene $\delta^{18}O_{lw}$ values were superimposed by lower values at ca. 6.5 cal ka BP, interpreted as increased winter precipitation contributing to snowmelt and isotopically light groundwater impacting $\delta^{18}O_{lw}$. This interval is coupled with highly siliceous sediment deposition indicating marked aquatic productivity, possibly linked with inputs of groundwater rich in silica and phosphorous. Our findings underscore the importance of hydrological connectivity on both burial and sourcing of C in high-latitude lakes, and suggest that in future wetter climate, high-latitude lakes may play more important role as processors than sinks of carbon.

1. Introduction

Lakes are a key component of the global carbon (C) cycle, acting as long-term sediment C sinks and short-term atmospheric C sources (Cole et al., 2007; Tranvik et al., 2009). Arctic-boreal regions have the highest lake density worldwide (Verpoorter et al., 2014), with a quarter of the global lake area found between latitudes 60°N and 69°N (Downing et al., 2006). Recent rapid Arctic climate warming (England et al., 2021; Rantala et al., 2015), coupled with an intensified water cycle and increased precipitation (Rawlins et al., 2015; Bailey et al., 2021; McCrystall et al., 2021), is transforming catchment and lake characteristics, with repercussions on lake ecosystem functioning (Wrona et al.,

* Corresponding author.
E-mail address: lilia.orozco@helsinki.fi (L.E. Orozco).

https://doi.org/10.1016/j.quascirev.2025.109323
Received 18 September 2024; Received in revised form 14 March 2025; Accepted 20 March 2025
Available online 26 March 2025

2016; Anderson et al., 2020; Marttila et al., 2021; Saros et al., 2023) and landscape C cycling (Hanson et al., 2015; Casas-Ruiz et al., 2023). Climate warming is shown to increase primary production and in-lake (autochthonous) C supply (Smol et al., 2005; Rantala et al., 2015), while increased hydrological connectivity is expected to increase the relative role of land-derived (allochthonous) C in inland waters, leading to lake browning and promoting heterotrophy (Karlsson et al., 2009; Kuhn and Butman, 2021). In some northern high-latitude regions, increased evaporation and permafrost collapse are diminishing, rather than increasing, hydrological connectivity (Woolway et al., 2020; Webb et al., 2022), which may reduce allochthonous C contributions to lakes (Johnston et al., 2020). The specific impacts of Arctic hydroclimate change on lake carbon sourcing and burial, however, remain poorly understood. Recent studies indicate that the type of catchment vegetation plays an important role in how lake ecosystem responds to browning; in high Arctic tundra lakes allochthonous material supply has been shown to promote in-lake primary production (Ayala-Borda et al., 2021; Stevenson et al., 2021). Moreover, McGowan et al. (2018) demonstrate how the expansion of shrubs in sparsely vegetated Arctic tundra catchments led to small increases in allochthonous C inputs that provide photoprotection and promote aquatic production, while substantial land-derived C supply from forested catchments had an opposing impact.

Many of the climate-driven landscape-scale processes, including vegetation and soil development, and catchment hydrological connections, unfold over long time scales and are difficult to trace solely by (field or satellite) monitoring of modern environments. Moreover, northern high-latitude lake C stores (sediment deposits) accumulated continuously over the Holocene (past 11.7 ka BP), following the retreat of continental ice sheets (Johansson, 1995; Stroeven et al., 2016). Therefore, they offer unique natural archives for studying the impact of past climate and land-cover changes on lake C sources and burial (e.g. Anderson et al., 2009; Balascio et al., 2020). In northern Europe, millennial-scale Holocene temperature trends are relatively well-known: an early Holocene warming, followed by the Holocene Thermal Maximum (HTM) between around 8-4 cal ka BP with temperatures up to 2 °C warmer than at present, and late Holocene cooling after ca. 5-4 cal ka BP until the 20th century (Mayewski et al., 2004; Seppä et al., 2009; Renssen et al., 2012; Mauri et al., 2015; Sejrup et al., 2016). Temperature trends were driven by orbitally forced northern hemisphere insolation changes and internal feedbacks from cryospheric, oceanic and atmospheric systems (Renssen et al., 2012; 2012). Holocene hydroclimate changes (precipitation, moisture balance) and their impacts on hydrological connectivity are more difficult to reconstruct and thus less well known in this region, but reconstructions generally indicate wetter conditions in the early Holocene, a drier HTM and increased effective moisture in the late Holocene (Seppä and Hammarlund, 2000; Heikkilä et al., 2010; Balascio et al., 2020). Stable isotope values of oxygen ($\delta^{18}O$) and hydrogen ($\delta^{2}H$) are excellent indicators of changes in the water cycle (Gat, 1996; Bowen et al., 2019), and past lake water isotopic composition can be reconstructed from $\delta^{18}O$ or $\delta^{2}H$ in sediment compounds formed in past lake water, including authigenic carbonate (Talbot, 1990; Hammarlund et al., 2003), leaf waxes (Sachse et al., 2012) or chironomid head capsule chitin (Wooller et al., 2004; Verbruggen et al., 2011; Lamb et al., 2024). Lake water isotope composition, in turn, is dependent on changes in seasonal precipitation over summer and winter months, evaporative enrichment, and lake hydrology (Jonsson et al., 2010; St. Amour et al., 2010; Corcoran et al., 2021; Kjellman et al., 2022). Responses of lakes and catchments to hydroclimate changes over the past millennia have the potential to decipher future shifts in lake C cycling under a warmer and wetter north European climate (Ruosteenoja et al., 2020; Trancoso et al., 2024).

In this paper, we present Holocene sediment records of organic C burial and sources to Lake Kuutsjärvi, a small lake in northern Fennoscandia, together with a Holocene lake water $\delta^{18}O$ ($\delta^{18}O_{lw}$) reconstruction. We aim to disentangle the linkages of hydroclimate changes, sediment C burial and the relative contributions from autochthonous and allochthonous C sources. We calculated C burial rates, supplemented with a ground penetrating radar (GPR) survey of the basin sediments. Elemental (C, N) and stable isotope ($\delta^{13}C$, $\delta^{15}N$) measurements of modern catchment and lake vegetation and particulate organic matter (POM) were used as tracers to quantify and classify C sources, and to estimate source contributions through the Holocene using a Bayesian end-member mixing model. Parallel hydroclimate changes were inferred from a $\delta^{18}O_{lw}$ reconstruction based on fossil chironomid head capsules ($\delta^{18}O_{ch}$), supported by the characterization of modern lake isotope hydrology and Holocene chironomid species assemblages. Based on this data, we identify changes in the quantity and quality of sediment C inputs over the Holocene and discuss the influence of catchment and hydroclimate development on long-term C cycling and burial.

2. Materials and methods

2.1. Study site

Lake Kuutsjärvi (67°44′49″N, 29°36′36″E, 341 m a.s.l.) was formed shortly after the Fennoscandian Ice Sheet retreated west of the Värriötunturit low mountain chain (Johansson, 1995; Stroeven et al., 2016; Bogren, 2019). It is located in a sheltered valley formed over several stages of sub- and proglacial erosion by glacier meltwaters, inside the Värriö Strict Nature Reserve in north-eastern Finland (Fig. 1). The lake is a small (ca. 0.7 ha surface area, ca. 8 m deep), mesotrophic (total phosphorous, 13–26 μg l^{-1} and total nitrogen, 67–152 of μg l^{-1}) and clear (Secchi depth 8 m, i.e. to the bottom) headwater lake with a small (<1.5 km^2), steep catchment and a reduced littoral zone (Milardi et al., 2019) (Fig. 1C and D). It is a dimictic (Kuittinen, 2021), hydrologically open system with groundwater input, and has a short water retention time (<2 months). The lake is typically ice-covered from late October to late May, and the spring overturn typically starts beneath the ice cover (Kuittinen, 2021). Värriö Strict Nature Reserve is located within the northern boreal vegetation zone, however, subarctic tundra is present in the catchment at altitudes above ~400 m a.s.l. (Fig. 1B and C) (Mäkisara et al., 2019). The vegetation in the Lake Kuutsjärvi catchment consists mainly of sparse Scots pine (*Pinus sylvestris*) and Norway spruce (*Picea abies*) forests.

2.2. Lake basin morphology

The basin morphology and sediment distribution were surveyed in winter 2023 with a MALÅ Ramac ProEx Ground Penetrating Radar (GPR), using a setup with unshielded antennas of 50 MHz and 100 MHz. The antennas were towed in a dense network over the frozen lake, resulting in 58 parallel profiles (Fig. S1). The acquired GPR profiles were processed with the software Relfexw (Sandmeier) following standard procedures including amplitude corrections, time to zero correction and topographic and velocity corrections (Neal, 2004). The velocity corrections were calibrated using data of the lake water depth and sediment thickness from previously drilled sediment cores (Bogren, 2019). Based on the calibration, the velocities for the electromagnetic waves were 0.034 m ns^{-1} and 0.06 m ns^{-1} for water and the basin lake sediments (gyttja), respectively. Additionally, a basic velocity of 0.1 m ns^{-1} (Neal, 2004) was used for the basin sediments (glaciofluvial materials and till). The topography was corrected with a 2-m resolution LiDAR digital elevation model (DEM) (National Land Survey of Finland, 2014). The profiles with a disrupted GPS signal from the GPR were relocated as 2D cross-sections and used as input in the 3D model (Fig. S2). The 3D model was constructed with Leapfrog Geo (Seequent) comprising of four units: water, lake sediment, basin sediment and bedrock.

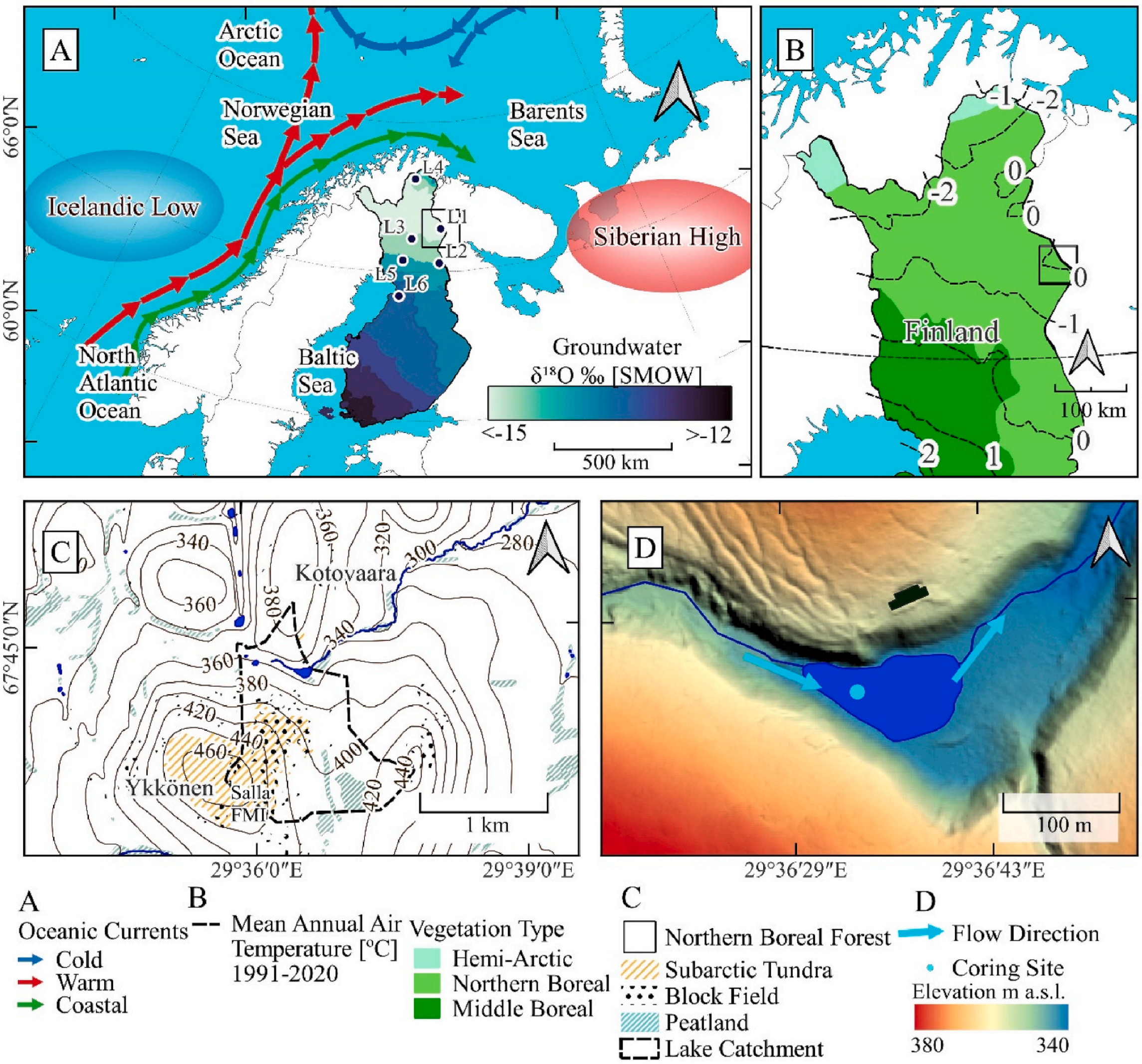

Fig. 1. Location map of the study site, with the location of the Värriö region denoted as a square (not to scale) in panels A and B. **A.** The main oceanic currents and atmospheric pressure centers influencing the climate, the variation in groundwater $\delta^{18}O$ in Finland (adapted from Kortelainen et al., 2004), and the reference sites for $\delta^{18}O$ in precipitation in northern Finland (L1 to L6 are Värriö, Oulanka, Sodankylä, Kevo, Rovaniemi and Oulu, respectively). **B.** Vegetation zones (data from Finnish Meteorological Institute, 2022) and the mean annual temperature (°C) for the normal period 1991–2020 (data from Finnish Meteorological Institute, 2022). The black square denotes the broader area around Värriö region. **C.** Local topography and land cover, Kuutsjärvi (center of the map) and its catchment area and the location of the meteorological station (Salla FMI) (contains data from the National Land Survey of Finland Topographic Database). **D.** Digital Elevation Model (DEM) for the lake surroundings (National Land Survey of Finland, 2014), the sediment coring site, and the Värriö Subarctic Research Station (black square) by which the precipitation sampler was located.

2.3. Modern reference material for isotope hydrology and carbon sources

The isotope hydrology of Lake Kuutsjärvi was monitored from November 2020 to February 2022. Lake surface-water samples were collected weekly during the ice-free season (from the first week of June 2021 to the last week of October 2021) and monthly during the ice-covered season. Shortly after the ice breakup in June 2021, a vertical profile of lake water, at a sampling interval of 1 m, was collected with a Limnos water sampler to gain insight into the lake-water $\delta^{18}O$ composition during the active season of the chironomid larvae (Danks and Oliver, 1972; Butler and Braegelman, 2018). The lake-water temperature profile was measured simultaneously. Local groundwater (pumped for household use at the research station) was sampled in summer (June 2021) and winter (February 2022). Local precipitation was collected once a month using a precipitation sampler designed to avoid evaporation (Gröning et al., 2012). All water sample vials were filled to the brim to avoid evaporation effects, kept in 30-ml HDPE bottles, and stored at 4 °C at the research station until further analyses. The samples were retrieved from the station and analyzed twice during the two-year monitoring period. The surface sediments (first cm) and the sediment-water interface were collected with an HTH gravity corer (Renberg and Hansson, 2008) in June 2021, from two deep sites and two shallow sites for analyzing head-capsule $\delta^{18}O$ of the modern chironomid larvae populations.

Terrestrial and aquatic vegetation from the catchment and lake were collected in June 2020 and June 2021. The samples consist of common plant species in the lake catchment and shoreline, as well as abundant aquatic mosses and epipelic algae growing at the lake bottom. Particulate OM from the lake was sampled in June 2020 by filtering lake water pooled from four water column depths onto borosilicate (GF/F, pore size 0.7 µm) filters. Up to 6 l of water was pumped per filter until the filter showed coloring. The vegetation samples were stored frozen prior to freeze-drying, grinding and analyses, while the filters were oven dried.

2.4. Sediment sampling, dating and chronology

Two full-length Holocene sediment core sequences (KJ1 and KJ2; ca. 1 m distance from each other) were collected with a heavy PP-piston corer (length 2 m, diameter 6 cm) (Putkinen and Saarelainen, 1998) from the deepest part of the lake (Fig. 1D) in April 2016 (Bogren, 2019; Salonen et al., 2024). The sequence KJ1 was 541 cm long and was analyzed using an ITRAX XRF core scanner with a Mo tube set at 30 kV and 50 mA, a dwell time of 35 s and a step size of 1.5 mm for core correlation. The cores were subsampled at 1-cm resolution and kept in cold storage (4 °C) until analysis. Subsamples at every depth were used for loss-on-ignition (LOI) at 550 °C (Heiri et al., 2001). Sediments on average at 5-cm intervals were sampled for elemental and stable isotope compositions of organic C and N, and at 4-cm intervals for chironomid species identification. Chironomid head capsules for chitin $\delta^{18}O$ analyses were picked at 10-cm intervals; if head capsules from the subsample did not yield a sufficient mass required for the $\delta^{18}O$ analysis, subsamples from adjacent depths were included.

The age-depth model for Lake Kuutsjärvi is published by Salonen et al. (2024) (Fig. S3). The chronology is based on 23 radiocarbon dates of terrestrial macrofossils (Table S1), and a Bayesian age-depth algorithm Bacon (Blanchet et al., 2022; Blanchet et al., 2022) modeled in R (R Core Team, 2022).

2.5. Elemental content and isotope composition of organic carbon and nitrogen

Modern plant, POM, and bulk sediment samples were measured for elemental content of organic C and N, and their stable isotope composition ($\delta^{13}C$, $\delta^{15}N$). Vegetation samples (consisting solely organic C) and sediment samples for $\delta^{15}N$ analyses were freeze-dried, ground to powder, and packed in tin capsules prior to measurements. Acid pretreatment has reported to have an influence on $\delta^{15}N$ values (Brodie et al., 2011b), and thus sediment $\delta^{15}N$ was analyzed on non-acidified samples separately from sediment $\delta^{13}C$. Sediment samples for dual elemental C:N and $\delta^{13}C$ analyses were rinsed with 10 % hydrochloric acid (HCl) to remove inorganic C (Brodie et al., 2011a). After ca. 24 h of constant shaking in HCl, the acids were decanted, and the samples were rinsed with deionized water until neutral. The samples were freeze-dried and packed in tin capsules for measurement. The samples were analyzed with a NC2500 elemental analyzer coupled to a Thermo Scientific Delta V Plus isotope ratio mass spectrometer at the Laboratory of Chronology, Finnish Museum of Natural History (LUOMUS). Triplicates were run for every 15 samples, and duplicates for every five samples. The isotope value reported for those results was the average of the repeats. The isotope data are expressed using standard delta notation, in per mil (‰) relative to international standards: Vienna Peedee Belemnite for C (VPDB), and atmospheric nitrogen (AIR) for nitrogen. The isotope values were calibrated with certified reference materials (USGS-40, USGS-41, IAEA-N1, IAEA-N2 for N, and USGS-40, USGS-41, IAEA-CH6 [ANU] and IAEA-CH7 for C). Repeated measurements of quality control materials (high organic sediment, corn leaf powder) showed a reproducibility of within ±0.2 ‰ for $\delta^{13}C$ and within ±0.1 ‰ for $\delta^{15}N$. Uncertainties expressed as the average standard deviation of the repeated subsample analyses were ±0.09 ‰ and ±0.04 ‰ for $\delta^{13}C$ and $\delta^{15}N$, respectively.

The POM samples were analyzed in quintuples and the plant samples in duplicates at the Stable Isotope Facility of the University of California, Davis, with a PDZ Europa ANCA-GSL elemental analyzer coupled to a PDZ Europa 20-20 isotope ratio mass spectrometer (EA-IRMS). The data were normalized to laboratory reference materials (alfalfa flour, amaranth flour, caffeine, chitin, glutamic acid, keratin, and nylon powder; calibrated against IAEA-600, USGS-40, USGS-41, USGS-42, USGS-43, USGS-61, USGS-64, and USGS-65) with the laboratory accuracy within ±0.02 ‰ for $\delta^{13}C$ and ±0.03 ‰ for $\delta^{15}N$. Uncertainties calculated from sample repeats were ±0.14 ‰ and ±0.17 ‰ for $\delta^{13}C$ and $\delta^{15}N$, respectively.

To compensate for the potential bias from the anthropogenic C emissions on the $\delta^{13}C$ values of materials younger than ca. 100 years, the samples were corrected for the Suess effect (+2 ‰) (Dombrosky, 2020). The correction affected only the vegetation samples, as the sediment chronology starts at 146 cal a BP, before the industrial revolution.

2.6. CAR calculation

The C accumulation rate (CAR) was calculated as a product of the sedimentation rate (cm a^{-1}), the sediment organic C content (C %), and the dry bulk density (g cm^{-3}). The dry bulk density was calculated from the ratio of the wet sediment weight and the dry weight, and their product with the wet density. The wet density ρ_w (Eq. (1)) was estimated without volumetric measurements considering the density of solid particles (ρ_m) of 2.6 g cm^{-3} in Finnish lake sediments (Pajunen, 2000). Organic content was derived from LOI, and water content from drying at 105 °C. The CAR was calculated at intervals of 500 years.

$$\rho_w = \frac{100^*\rho_m}{100 + 1.6(W + LOI)(\rho_m - 1)} \ldots Eq.1$$

A constrained cluster analysis of the sediment accumulation rate, C:N ratio (wt %), $\delta^{13}C$ and $\delta^{15}N$ data was performed to define temporally divergent zones of OM sedimentation, using the *rioja* package (Juggins, 2019) and euclidean distance method in R 4.1.3 (R Core team, 2022). The millennial-scale trends in the OM composition were examined with generalized additive models (GAM). The GAM models for C %, N %, C:N ratio, $\delta^{13}C$ and $\delta^{15}N$ were calculated using the package *mgcv* (Wood, 2017) in R 4.1.3 (R Core Team, 2023), using the Restricted Maximum Likelihood (REML) method for smoothness fitting. The parameters for the number of *basis* functions (knots, $k = 50$) and smoothness ($\lambda = 0.01$) were determined visually by trial and error considering the number of data points and the fit of the model, avoiding overfitting while capturing the temporal shifts in the geochemical records.

2.7. δ^2H and $\delta^{18}O$ of modern water samples

Stable isotope compositions (δ^2H and $\delta^{18}O$) of precipitation, lake water, and groundwater samples were analyzed in duplicates with a Picarro Isotopic H_2O L115-I analyzer at the Helsinki Geoscience Laboratories, Department of Geosciences and Geography, University of Helsinki. The measurements were normalized with laboratory standards W-5 ($\delta^2H = -72.9$ ‰, $\delta^{18}O = -9$ ‰), W-7 ($\delta^2H = -158.9$ ‰, $\delta^{18}O = -21.2$ ‰), and W-118 (quality standard, $\delta^2H = -73.2$ ‰, $\delta^{18}O = -9.1$ ‰), calibrated against Vienna Standard Mean Ocean Water (VSMOW) and Standard Light Antarctic Precipitation (SLAP) with a laboratory accuracy of ±0.4 ‰ and ±0.07 ‰ for δ^2H and $\delta^{18}O$, respectively. Uncertainty based only on sample replicates was ±0.4 ‰ and ±0.03 ‰ for δ^2H and $\delta^{18}O$, respectively. The results are reported relative to VSMOW. The δ^2H and $\delta^{18}O$ of precipitation were used to calculate a local meteoric water line (LMWL) for the Värriö region. The variation in δ^2H and $\delta^{18}O$ in precipitation and lake water was assessed against the changes in air temperature, snow depth, and precipitation amount recorded at the meteorological station at Salla Värriötunturi (Fig. 1C) during the monitoring period, and against the 1991–2020 climate normals (Finnish Meteorological Institute, 2022). Thermal seasons were defined according to the Finnish Meteorological Institute (2022): spring was a season when mean daily temperature rose continuously above 0 °C, summer when mean daily temperature rose continuously above 10 °C, autumn when mean daily temperature lowered continuously below 10 °C, and winter when mean daily temperature was lowered continuously below 0 °C, respectively. The mean daily temperature to determine the change of season was calculated as a moving average for a 15-day period with the R package *zoo* (Zeileis et al., 2014) in R 4.1.3 (R Core Team, 2023).

2.8. End-member mixing model

The relative inputs of different sediment C sources through time were estimated with a Bayesian end-member mixing model (Parnell et al., 2010) using package *simmr* (Govan and Parnell, 2023) in R 4.1.3 (R Core Team, 2023). The package uses tracer data from a pool (mixture) and solves mixing equations to determine possible contributions from sources (end members). In this case, the tracers were C:N, $\delta^{13}C$, or $\delta^{15}N$, the mixtures were sediments, and the sources were derived from modern reference samples (terrestrial vegetation, aquatic POM, aquatic mosses, and benthic algae). The tracers and end members for the final model were selected based on the distribution of the sources and the mixtures in tracer biplots, allowing enough separation of end-member groups while enclosing the mixture group. In addition, previously reported source ranges were considered (Lamb et al., 2006; Riis et al., 2016; Thompson et al., 2018; Osburn et al., 2019). To discern millennial-scale trends in C source contributions, the model was run at intervals of approximately 1000 years considering the temporal zonation from the cluster analysis of sediment OM data. The model output for each mixture group was checked for diagnostics (convergence into a solution), and statistics (mean and standard deviation, prior vs. posterior data). The average posterior predicted value was considered as the relative proportional contribution of each end-member category to the mixture group.

2.9. Chironomid species assemblages and head capsule $\delta^{18}O$

For chironomid species identification, sediment samples were treated following established protocols (Brooks et al., 2007), with sediment samples dissolved in a 10 % potassium hydroxide (KOH) solution and heated on a hot plate for 10–20 min, before filtering through a 100-μm sieve. The sieved sediments were placed in a Bogorov counting plate under a stereomicroscope for isolating and cleaning the head capsules with precision tweezers. Finally, the head capsules were mounted on microscope slides with Euparal. The chironomid species and morphotype identification and ecological grouping (e.g. profundal and littoral), followed Schulze (1994), Brooks et al. (2007), Vallenduuk and Moller Pillot (2007), Moller Pillot (2009, 2014) and Andersen et al. (2013).

The chironomid head capsules chosen for oxygen isotope analysis ($\delta^{18}O_{ch}$) were handpicked from fresh sediments, rinsed only with deionized water following established protocols (Wooller et al., 2004; Verbruggen et al., 2011; Arppe et al., 2017). The cleaned head capsules (233 ± 99 head capsules per sample) were weighed (80 ± 20 μg per sample) into silver capsules and freeze-dried prior to analyses with a TC/EA coupled to a Thermo Finnigan Delta V Advantage IRMS, via a ConFlo III interface, at the Stable Isotope Biogeochemistry Laboratory (SIBL), Durham University. The measurements were calibrated with IAEA international standards (600–602, CO-9, SO-5, SO-6), with an internal laboratory precision of ±0.2 ‰. The data is reported relative to VSMOW.

The biological fractionation factor, i.e., the conversion from

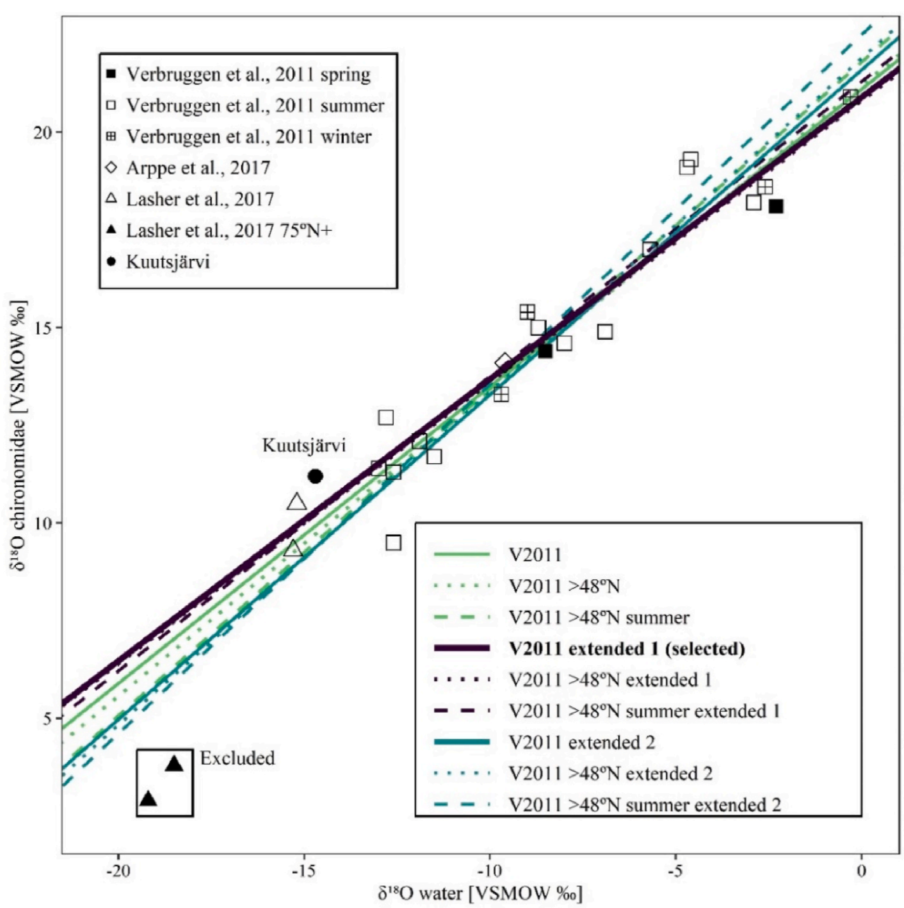

Fig. 2. Alternative calibrations considered for the reconstruction of $\delta^{18}O_{lw}$ from $\delta^{18}O_{ch}$. The original Verbruggen et al. (2011) calibration is labeled V2011 (pale green line). V2011 > 48°N = V2011 calibration with only the northern lakes (assumed in the range of Värriö area climates during the Holocene), V2011 > 48°N summer = V2011 calibration with only the northern lakes sampled in summer, extended 1 = calibration data from the other northern lakes (present work, Arppe et al., 2017; Lasher et al., 2017) but excluding the two outliers (Lakes Stardam and Secret), extended 2 = calibration data from other northern lakes, including Lakes Stardam and Secret.

measured $\delta^{18}O_{ch}$ to past lake water oxygen isotope composition ($\delta^{18}O_{lw}$), was calculated using the linear relationship between $\delta^{18}O$ values in lake water and surface-sediment chironomid head capsules. The conversion was based on the original European dataset by Verbruggen et al. (2011), with additional data available for northern high-latitude lakes: Lake Kuutsjärvi, Lake Svartvatnet in Svalbard (Arppe et al., 2017), and Lakes Stardam, Secret, T1 and T2 in northwest Greenland (Lasher et al., 2017) (Table S2). We explored several alternatives for the calibration (Fig. 2, Table S3). The dataset of Verbruggen et al. (2011) contains lakes located in southern European climatic settings not representative of the range of Värriö climates over the Holocene. Thus, we explored calibration alternatives excluding the lakes located south of 48°N. Moreover, we tested a calibration alternative with only the lakes sampled in summer to account for possible seasonal bias. The different alternatives of the Verbruggen et al. (2011) dataset did not introduce marked differences to the $\delta^{18}O_{lw} - \delta^{18}O_{ch}$ calibration (pale green lines in Fig. 2). However, the Lasher et al. (2017) Lakes Stardam and Secret at 75 °N in Greenland stand out as outliers in the calibration data and including them in the regression (option “extended 2”) leads to markedly higher reconstructed $\delta^{18}O_{lw}$ in the lower (“colder”) end of the calibration range and lower values in the higher (“warmer”) end, respectively (dark green lines in Fig. 2). In the absence of more calibration data from the coldest end of the spectrum, we decided to exclude Lakes Stardam and Secret from the calibration. Based on these explorative analyses, the final selected $\delta^{18}O_{lw}$–$\delta^{18}O_{ch}$ calibration included the full Verbruggen et al. (2011) set and the other northern high-latitude lakes excluding Lakes Stardam and Secret (calibration “V2011 extended 1”, Fig. 2):

$$\delta^{18}O_{ch} = 0.72\delta^{18}O_{lw} + 20.9 \tag{2}$$

$R^2 = 0.90$ All the equations for the regression lines (Fig. 2) are presented in the Appendix (Table S3). The reconstructed values were modeled with GAMs to evaluate trends in Holocene $\delta^{18}O_{lw}$ using methodology similar to that for the OM data. The model parameters were 18 knots and 0.1 smoothness and were determined per trial and error as for the OM GAMs.

3. Results and discussion

3.1. Lake basin morphology and sedimentation rate

The GPR data shows that Kuutsjärvi lake sediments accumulated in a steep-walled bedrock basin, which is the deepest in its western end (Figs. S1 and S2). The bedrock basin is overlain by (south)eastward thickening Quaternary glaciofluvial and till deposits (Fig. S2). The lake sediment (gyttja) accumulation is focused on the (north)western part of the lake by the sediment coring location, where the thickest gyttja layers are found (Fig. 3). The lake basin morphology was likely shaped by the eroding impact of meltwaters from the northwestwards receding Fennoscandian Ice Sheet (Johansson, 1995). The meltwaters from the west pushed the loose Quaternary deposits eastwards. There is stratigraphic evidence (Bogren et al. 2019; Salonen et al., 2024) of two high-energy, early-Holocene meltwater overflow events in the minerogenic sequence deposited prior to the lake sediment gyttja section studied here (see Bogren, 2019; Salonen et al., 2024).

The age-depth model of Lake Kuutsjärvi is well-constrained and follows a quasi-linear trend throughout the early and mid-Holocene (Fig. S3; Salonen et al., 2024), with an average sediment accumulation rate of 0.083 cm a^{-1}. There is an inflection point in the age-depth curve at ca. 3.8 cal ka BP, with subsequent decline in the sedimentation rate to 0.015 cm a^{-1}. The change in the sedimentation rate could be largely explained by the basin morphology. The initially small and steep basin was first infilled with sediment, after which the area of accumulation became much larger (Fig. 3; Figs. S1 and S2), decreasing sediment accumulation rate at the coring location. Bennett and Buck (2016) proposed such conceptual model for sedimentation curves, demonstrating that when a funnel-shaped lake has filled to a point where the basin is flatter, the sedimentation rate slows down. Increasing throughflow could have flushed OM out of the lake basin and slowed down the sedimentation. Thus, the slower sedimentation rate from ca. 3.8 cal ka BP onwards could be due to combined effects from basin morphology (a change in sediment distribution) and changes to catchment C flow (balance between OM inputs and outputs to the basin).

3.2. $\delta^{18}O_{ch} - \delta^{18}O_{lw}$ calibration and reconstruction

The past $\delta^{18}O_{lw}$ values in this study were reconstructed from $\delta^{18}O$ in

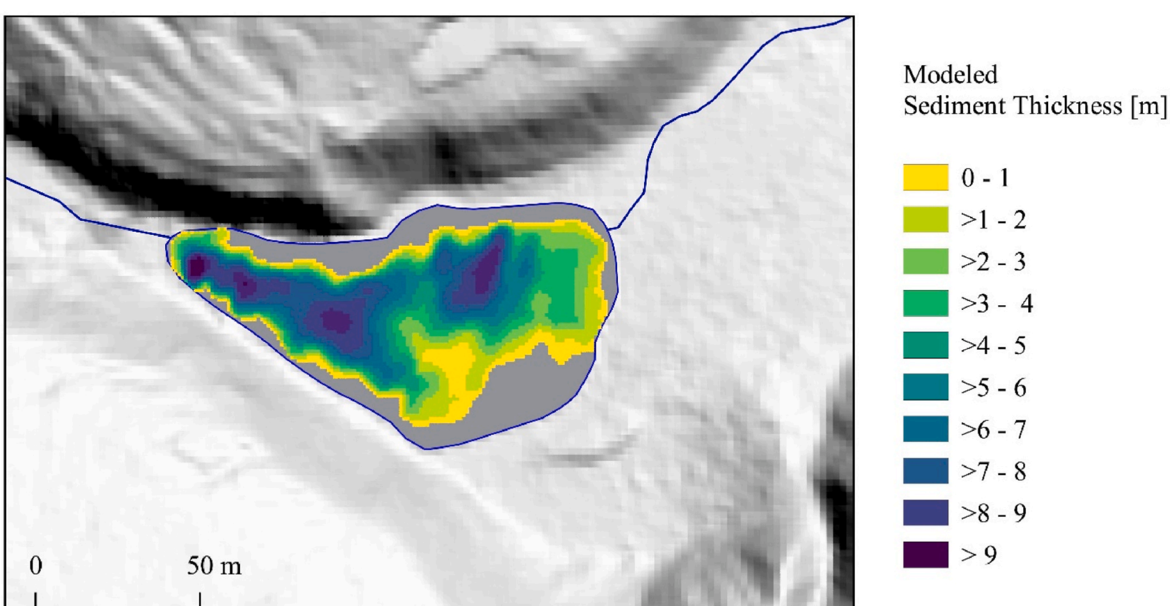

Fig. 3. Modeled thickness of the lake sediment (gyttja) layer based on the Kuutsjärvi GPR data.

chitinous head capsules of the fourth instar of chironomid larvae, which most circumpolar species reach in summer (Oliver, 1968; Danks, 1971; Walker, 1987; Butler and Braegelman, 2018; Lackmann and Butler, 2018). The oxygen isotope composition of head capsules of chironomid larvae ($\delta^{18}O_{ch}$) is an established proxy for $\delta^{18}O_{lw}$ (Wooller et al., 2004; Verbruggen et al., 2011; Lamb et al., 2024). The reconstructed $\delta^{18}O_{lw,}$ in turn, reflects regional hydroclimate and lake hydrology. Generally, $\delta^{18}O_{lw}$ tracks that of rainfall, while air temperature is often the predominant driver of precipitation $\delta^{18}O$ in high-latitude environments (Dansgaard, 1964; Rozanski et al., 1993). In addition, $\delta^{18}O_{lw}$ may be altered by evaporation at the lake surface during the open-water season, groundwater influence, or seasonal events such as spring snowmelt. To assess these impacts, we measured precipitation, lake water and groundwater isotope composition at the study site (see Appendix A for complete results and discussion). At present, Lake Kuutsjärvi is an open groundwater-influenced system, and the seasonal variation in $\delta^{18}O_{lw}$ during the monitoring period was conspicuously small (within 0.3 ‰ for $\delta^{18}O$; Tables S5 and S6). Supplementary Fig. S4E shows Kuutsjärvi lake water $\delta^{18}O$ and $\delta^{2}H$ plotting parallel to and above the local mean water lines (LMWLs) for northern Finland, suggesting that lake water is not affected by evaporation and is biased towards ^{18}O depleted winter precipitation and snowmelt. Värriö groundwater displays typical seasonal attenuation of precipitation composition: depletion from previous winter's snowmelt in early summer ($\delta^{18}O = -15.1$ ‰), and plotting closer to the precipitation of the previous open-water season in February ($\delta^{18}O = -14.2$ ‰) (Fig. S4E). In early summer during the chironomid larval activity, groundwater impact is also reflected in the lake water, and the isotopic composition of the water column is vertically stable (Table S7). Thus, the $\delta^{18}O_{ch}$ based Holocene $\delta^{18}O_{lw}$ reconstruction can be interpreted as cold-season biased mean annual precipitation $\delta^{18}O$ as long as the lake hydrological setting remained similar.

The reconstructed modern $\delta^{18}O_{lw}$ value of -13.5 ‰ (using Eq. (2)) from surface sediment $\delta^{18}O_{ch}$ collected in 2021 is 1 ‰ higher than the measured Kuutsjärvi $\delta^{18}O_{lw}$ during the ice-free period (June–October 2021, -14.5 ± 0.1 ‰) (Fig. 4, top panel). Applying any other calibration set (Fig. 2) would lead to an even larger difference. The inaccuracy in the calibration models could be due to the different temporal coverages of the lake water and chironomid samples, the latter encompassing only one season, and the former representing surface sediment deposited over several years. Another reason could be a habitat bias in the European calibration set, comprising surface waters sampled mostly in summer (Verbruggen et al., 2011; Arppe et al., 2017; Lasher et al., 2017), potentially affected by surface evaporation during thermal stratification, that was not influencing the chironomid larvae that were sampled from lake bottoms. Lake Kuutsjärvi, in turn, appears isotopically well-mixed in June, with similar $\delta^{18}O_{lw}$ values in the surface and bottom waters (Table S7). Altogether, the differences in the seasonal sampling times and the limited calibration data from the Arctic adds to the inaccuracy of the calibration models. Addressing these gaps in understanding would greatly advance high-latitude $\delta^{18}O_{lw}$ reconstructions (see also recommendations by Lamb et al., 2024). Here, given the differences between measured and reconstructed modern $\delta^{18}O_{lw}$, the Holocene $\delta^{18}O_{lw}$ trends, rather than absolute values, are used for past hydroclimate interpretation.

The reconstructed Holocene $\delta^{18}O_{lw}$ mirrors the overall air temperature development in the region (Shala et al., 2017; Lenz et al., 2021; Krikunova et al., 2022; Otiniano et al., 2024; Salonen et al., 2024), gradually increasing in the early Holocene, reaching maximum values in the mid-Holocene, and dropping subsequently in the late Holocene (Fig. 4). Recent research suggests a small (ca. -0.1 ‰ per °C) temperature-dependent fractionation effect between oxygen isotopes in chitin and lake water (Lombino et al., 2021), implying that lake water warming increasingly favors the incorporation of ^{16}O in chironomid chitin, leading to lower $\delta^{18}O_{ch}$. The fractionation can thus cause attenuation of the climatic signal incorporated in $\delta^{18}O_{ch}$ because temperature shifts have an opposing impact on precipitation $\delta^{18}O$ (climate warming leads to precipitation more enriched in ^{18}O), and thus the amplitude of changes in the Kuutsjärvi Holocene $\delta^{18}O_{lw}$ maybe underestimated.

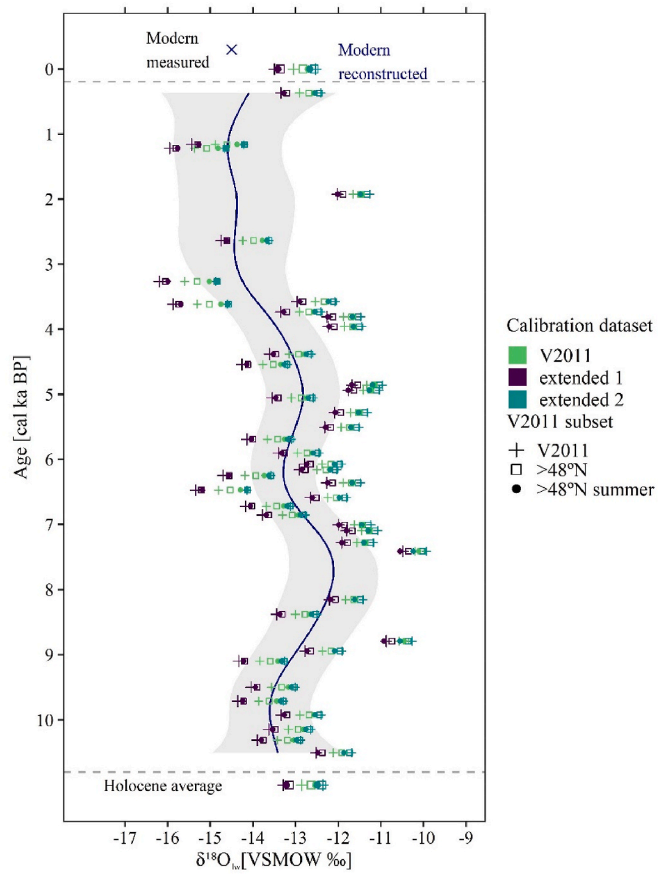

Fig. 4. Alternative Lake Kuutsjärvi $\delta^{18}O_{lw}$ reconstructions using the $\delta^{18}O_{lw}$–$\delta^{18}O_{ch}$ calibrations presented in Fig. 2. The reconstructed Holocene values with the chosen calibration (V2011 extended 1) are marked with dark purple crosses, and are smoothed with generalized additive model (GAM, dark blue line). The top of the panel shows the modern measured (average June–October) and reconstructed (based on $\delta^{18}O_{ch}$ from surface sediments collected in June 2021) $\delta^{18}O_{lw}$ values, and at the bottom are the reconstructed Holocene average $\delta^{18}O_{lw}$ values.

It is assumed that ca. 70 % of the oxygen in chitin derives from the water the chironomid larvae live in, and the remaining 30 % from their diet (Wang et al., 2009; Soto et al., 2013) and that there are no major differences in oxygen isotope fractionation between species (Verbruggen et al., 2011). However, recent research demonstrates potential taxon-specific fractionation effects on oxygen isotopes incorporated in chitin (Chang et al., 2018), and single-taxon isotope analysis can help eliminate this bias (van Hardenbroek et al., 2018; Lamb et al., 2024). To reach the required sample yield for the $\delta^{18}O_{ch}$ analysis of Lake Kuutsjärvi, it was necessary to use mixed species assemblages. However, while the chironomid species assemblages show some changes in the proportional contributions of species over the Holocene, the main chironomid taxa remain the same (Fig. S5). We thus assume that species-specific fractionation did not inflict a notable bias on Lake Kuutsjärvi $\delta^{18}O_{lw}$ record. The dominant chironomid taxa are cold stenotherm species and profundal dwellers (e.g. *Heterotrissocladius* spp., *Sergentia coracina* -type, *Tanytarsus lugens* -type, *Micropsectra*-type *Heterotrissocladius grimshawi*; Brooks et al., 2007; Moller Pillot, 2009) (Fig. S5). Also, a small but consistent proportion of the taxa are related to seepages and springs suggesting groundwater influence on Lake Kuutsjärvi throughout the Holocene. Therefore, the chironomid assemblages support the notion that chitin-based Lake Kuutsjärvi $\delta^{18}O_{lw}$ records cold-season biased mean annual precipitation.

3.3. Modern organic matter sources

The three primary sources of OM to Lake Kuutsjärvi sediments (terrestrial, lake bottom and POM) were separated by their C:N and $\delta^{13}C$ values (Fig. 5; Fig. S6, Table S10). Nitrogen isotope composition, however, did not separate the OM sources (Fig. S6) and was not used in the end-member mixing model. Allochthonous terrestrial material had a C:N range from 12.3 to 59.8 (average 25.3 ± 11), and $\delta^{13}C$ range from −31.3 to −23.5 ‰ (average, −26.8 ‰ ± 1.3), equivalent to reported values from boreal and subarctic ecosystems (Fig. 5; Finlay and Kendall, 2007; Butterbach-Bahl et al., 2011; Burpee and Saros, 2020). Autochthonous sources were divided into two categories, lake bottom and POM, which were separated by their C:N ratios (Fig. 5). The lake bottom class comprises aquatic mosses and benthic algae with C:N ranging from 11 to 19.2 (average 15.1 ± 4), and $\delta^{13}C$ ranging from −33 to −37 ‰ (average −35.8 ± 1.8 ‰) (Fig. 6), where the C:N of aquatic mosses approaches that of terrestrial vegetation (Table S6). The POM filtered from the water column had a C:N range from 4.4 to 7.4 (average 6 ± 1.2), and a $\delta^{13}C$ range from −37.2 to −33.1 ‰ (average −35.5 ‰ ± 1.7) characteristic of freshwater algal production (Fig. 6; Lamb et al., 2006; Finlay and Kendall, 2007).

The lake bottom OM sources in Lake Kuutsjärvi have low $\delta^{13}C$ values relative to the literature range for submerged aquatic plants and benthic algae, which are typically separated from pelagic algal source by their higher $\delta^{13}C$ values (France, 1995). This is probably because most of the lake bottom samples are aquatic moss species (*Fontinalis* spp. and *Warnstorfia trichophylla*), which in the few reports from Arctic-boreal locations have relatively low $\delta^{13}C$ values (−34 to −24 ‰) (Riis et al., 2016; Thompson et al., 2018; McFarlin et al., 2023). The functional group is often decisive for the $\delta^{13}C$ values of aquatic vegetation, since it influences dissolved inorganic C type in the typical habitat and the physiological differences in the fractionation mechanisms(Chang et al., 2018; Thompson et al., 2018). Many aquatic mosses fix only dissolved aquatic CO_2 (Bain and Proctor, 1980; Riis and Sand-Jensen, 1997), explaining their generally low $\delta^{13}C$ values for a benthic habitat. In the end-member mixing model, autochthonous pelagic production (POM) and allochthonous sources are well-separated, while the lake bottom end member overlaps with POM with respect to $\delta^{13}C$, and with terrestrial material with respect to C:N. Thus, when accounting for both tracers, lake bottom source has its own fingerprint in the $\delta^{13}C$ – C:N space (Fig. 5). Our findings highlight that understanding the geochemical composition of the local aquatic vegetation is essential for accurate interpretation of OM sourcing. In typical high-latitude clear-water lakes, aquatic mosses and benthic algal mats form an essential but less well constrained C source, which may introduce a considerable bias in the interpretation of C sourcing due to the overlap with the literature values of pelagic production and even allochtonous OM.

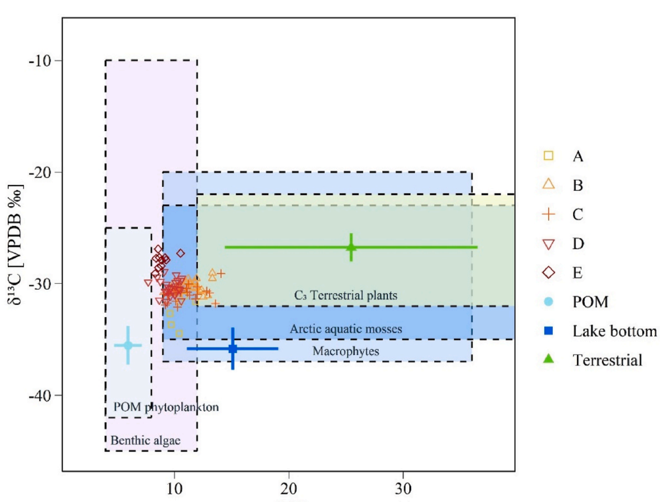

Fig. 5. End-member mixing model input data for sediment OM sources (modern samples, blue and green), shown as average values with standard deviations, and Holocene C:N and $\delta^{13}C$ values (yellow, orange and red symbols) as temporal zones A to E from the cluster analysis (see Fig. 6). The ranges in dashed boxes are values for OM sources from literature (Lamb et al., 2006; Finlay and Kendall, 2007; Riis et al., 2016; Thompson et al., 2018).

3.4. Holocene changes in sediment C burial

The cluster analysis applied to the OM data identified five zones (Fig. 6). Zones E (from 10.5 to 9.6 cal ka BP) and D (from 9.6 to 8 cal ka BP) will be here onwards referred to as the early Holocene, Zones C (from 8 to 5.8 cal ka BP) and B (from 5.8 to 3.1 cal ka BP) as the mid-Holocene, and Zone A (since 3.1 cal ka BP) the late Holocene). The range of Holocene CAR in Lake Kuutsjärvi (0.5–13.1 g C m^{-2} a^{-1}, average: 8.5 ± 4.3 g C m^{-2} a^{-1}) falls within what is reported for other lakes in Finland (1–23.7 g C m^{-2} a^{-1}; Pajunen, 2000) and in the circum-Arctic region (1.2–7.9 g C m^{-2} a^{-1} in northern Quebec; Ferland et al., 2012; 3.5–11.5 g C m^{-2} a^{-1} in southwestern Greenland, Anderson et al., 2009; and 3.5 g C m^{-2} a^{-1} in northern Siberia, Vyse et al., 2021). While the sediment accumulation rate, and thus the CAR, at the core location were heavily influenced by lake basin morphometry (Fig. 3, Figs. S1 and S2), Holocene changes in the amount of autochthonous and allochthonous contributions to Lake Kuutsjärvi appear to have an impact on the CAR as well.

The highest CAR values and slightly higher C:N values in the mid-Holocene coincide with the regional (Seppä et al., 2009; Sejrup et al., 2016) and the northeast Fennoscandian (Seppä et al., 2008; Shala et al., 2017; Lenz et al., 2021; Krikunova et al., 2022; Otiniano et al., 2024; Salonen et al., 2024) HTM at ca. 8–4 cal ka BP. A recent study of C burial over the past 21 cal ka BP in 28 lakes across the Arctic reports an overall increase in C accumulation during warmer periods, but the burial patterns in many of the lakes in the study are not explained by temperature (Pfalz et al., 2023). Carbon burial in Lake Kuutsjärvi was likely indirectly impacted by warming through changes to hydrological connectivity. The higher sediment TOC% during the HTM (Fig. 6) coincides with lake level lowering in northern Finland (Hyvärinen and Alhonen, 1994; Eronen et al., 1999; Korhola et al., 2005; Väliranta et al., 2015; Siitonen et al., 2011). Lake Kuutsjärvi has a shallow outlet, and it is likely that lake level lowering during the HTM closed the system, trapping the OM arriving to the lake and produced in the lake within the basin. In general, smaller and shallower lakes tend to have higher OM preservation potential and CAR values due to limited remineralization with less water column depth (Kortelainen et al., 2004; Ferland et al., 2012).

During the HTM, there are two CAR minima at ca. 8 and 6 cal ka BP, where sedimentation rate remains unchanged and sediment TOC% and C:N ratio decrease (Fig. 6). The periods coincide with continuous yellow laminations in the lithostratigraphy (Fig. 6), interpreted as periods of intense algal blooms consisting primarily of siliceous diatoms. The high sediment silica content could explain the lower proportion of C in sediment, and hence lower CARs at these times compared to the rest of the HTM. This interpretation is corroborated by the high dissolved Si concentrations in modern Lake Kuutsjärvi and the high contributions of amorphous silica from the catchment to recent lake sediments (Tallberg et al., 2015).

The markedly lower CARs in the late Holocene can be largely explained by sediment infilling at the coring location (see section 3.1) together with higher effective humidity contributing to hydrological opening and material escape from the lake. These changes were coupled by a general decrease in terrestrial productivity during the late Holocene cooling, seen as lowering TOC% and C:N values.

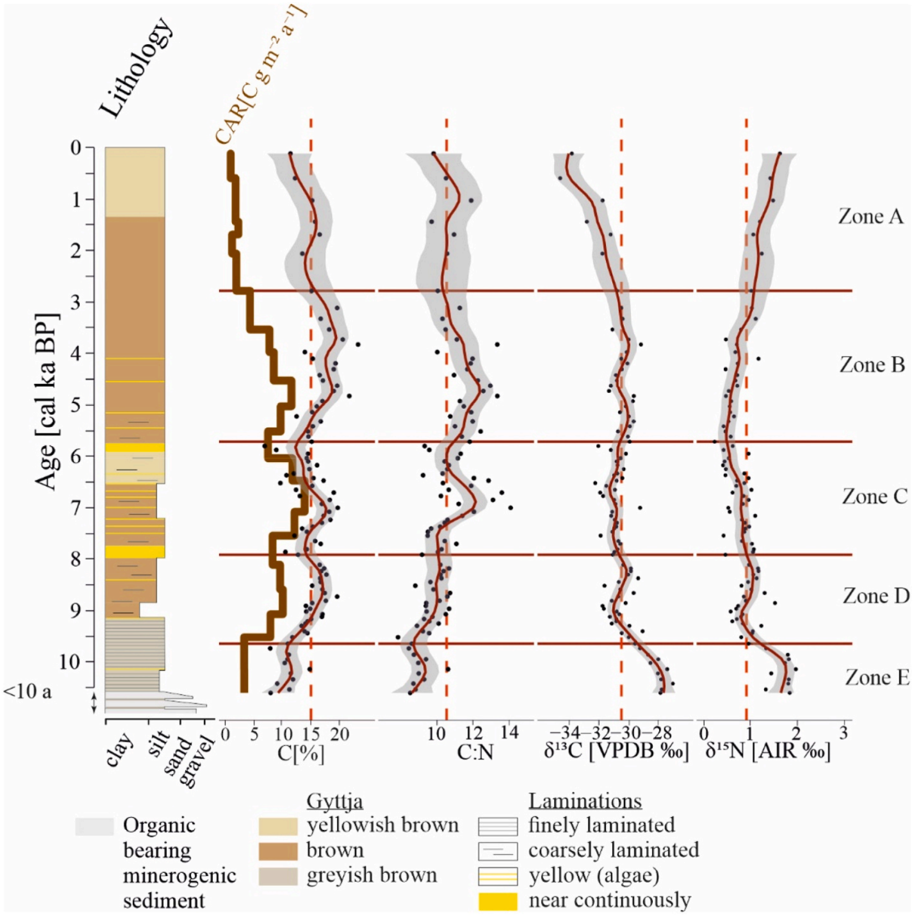

Fig. 6. Stratigraphic diagram with sediment organic geochemical data from Lake Kuutsjärvi. The zonation is based on cluster analyses. The geochemical sequences are smoothed with generalized additive models (GAMs; red line), and the Holocene average values are presented with a dashed line.

3.5. Holocene hydroclimate and sediment C sources

The Holocene CAR, the changes in TOC% and the OM source contributions follow the $\delta^{18}O_{lw}$ trends in Lake Kuutsjärvi (Fig. 7). The low $\delta^{18}O_{lw}$ values in the earliest and late Holocene are coupled with lower than average CAR (on average 3.2 g C m^{-2} a^{-1} in Zone A and E in comparison to the Holocene average of 9.2 g C m^{-2} a^{-1}) and C:N (8.8 and 10.7 for Zone A and E, respectively, in comparison to the Holocene average of 10.7; Fig. 6), suggesting lower C burial from mainly aquatic sources (Lamb et al., 2006; Meyers, 2003) during periods of higher effective moisture. This pattern is corroborated by the mixing model solution (Fig. 7C). Conversely, during the warmer and drier HTM with elevated $\delta^{18}O_{lw}$, the CAR and the C:N ratio are higher (CAR up to 13.1 g C m^{-2} a^{-1} and maximum C:N value 14 at ca. 6.9 cal ka BP; Fig. 6), indicating Holocene maximum C burial and above-average contribution from allochthonous sources, supported by the mixing model solution (Fig. 7C). These results are contrary to the expected increase in land-derived OM with hydrological connectivity (Blanchet et al., 2022).

It is likely that during the HTM, the higher $\delta^{18}O_{lw}$ resulted from both higher temperatures and surface evaporation. The shallow outlet of Lake Kuutsjärvi was likely at least periodically closed due to lake level lowering, which enhanced burial of incoming terrestrial material. Lake-level lowering during the HTM is observed in several northern Fennoscandian lakes (Eronen et al., 1999; Hyvärinen and Alhonen, 1994; Korhola et al., 2005; Siitonen et al., 2011). Furthermore, pine (*Pinus sylvestris*) tree line expanded northwards in Fennoscandia during the mid-Holocene (Seppä and Birks, 2001; Balascio et al., 2020). Around Kuutsjärvi, pollen and *seda*DNA records indicate dense catchment forest and nutrient-demanding field layer vegetation during the HTM; the maximum tree pollen proportion was reached around 7 cal ka BP (Salonen et al., 2024), coinciding with the sediment C:N maximum. Thus, landscape greening and C-rich forest soils over the HTM could have led to increased allochthonous C load contributing to higher sediment CAR in the (periodically) closed lake basin. Another explanation could be that the lake level lowering increased the area for shoreline vegetation which also have higher C:N values (Thompson et al., 2018), however, the littoral area of Lake Kuutsjärvi was likely marginal due to the steep morphology of the basin.

While the terrestrial OM contribution to Lake Kuutsjärvi increased during the HTM, also aquatic productivity was high and the burial of both autochthonous and allochthonous OM increased. The lower $\delta^{15}N$ values (Fig. 6), in turn, could be due to higher soil N content and contribution of terrestrial N to the lake, supporting aquatic productivity. Our results suggest that increased allochtonous inputs, or lake browning, did not hinder aquatic productivity in this forested lake setting. These findings demonstrate that hydroclimate influence on sediment C burial and sources in Lake Kuutsjärvi was mediated by the development of catchment vegetation and soils, nutrient inputs to the lake, and lake level lowering, which are more complex than expected from a simple change in hydrological connectivity.

An interesting feature of the Kuutsjärvi HTM is the dip in $\delta^{18}O_{lw}$ at around 6.5 cal ka BP, within the period of generally high $\delta^{18}O_{lw}$, which is coupled with fluctuations in the CAR, TOC% and OM sourcing. There is little indication of a mid-Holocene cold event in the regional summer temperature records (Lenz et al., 2021; Krikunova et al., 2022; Otiniano et al., 2024; Salonen et al., 2024). The HTM has generally been considered a stable warm period (Seppä and Birks, 2001; Sejrup et al., 2016; Otiniano et al., 2024), and the recent pollen-based July

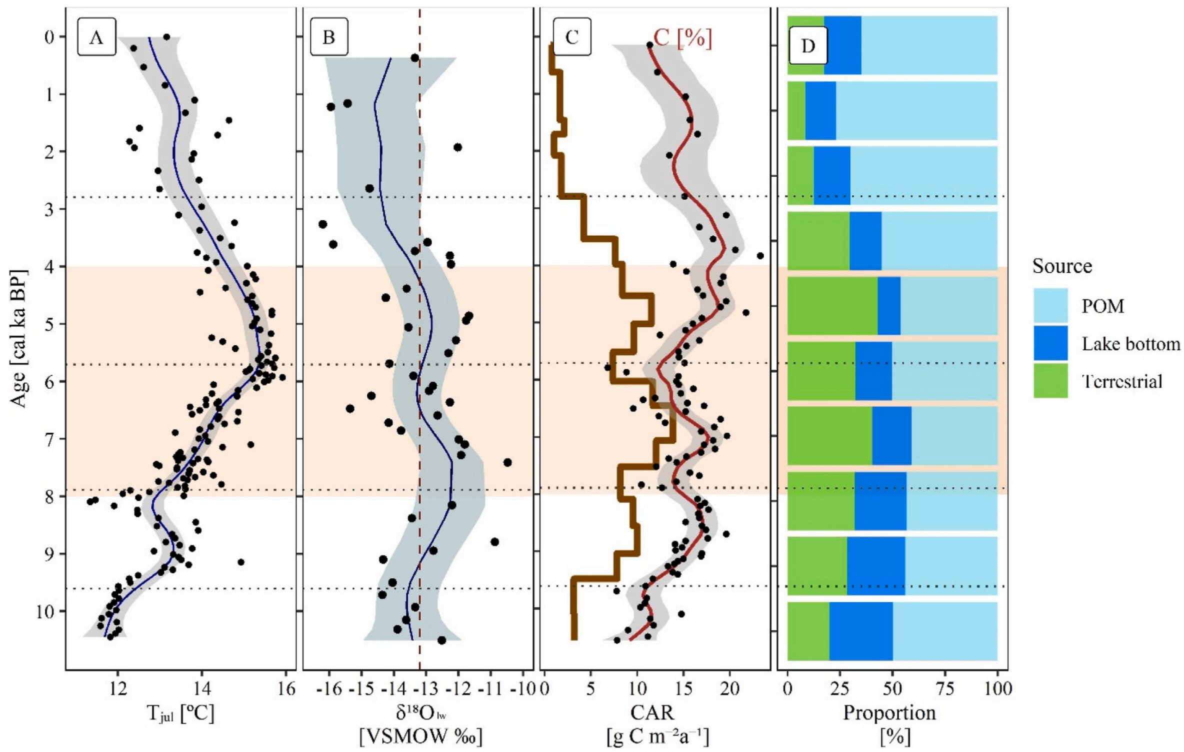

Fig. 7. **(A)** Pollen-based Holocene July temperature reconstruction (Salonen et al., 2024).**(B)** Holocene hydroclimate shifts as reconstructed by $\delta^{18}O_{lw}$ [VSMOW ‰]. The black circles correspond to the values calculated with Eq. (2), the data points are smoothed with generalized additive models (GAMs, blue line), Holocene average is marked with a dashed line. **(C)** Holocene sediment C quantity as the carbon accumulation rate (CAR) [g C m^{-2} y^{-1}] and the total organic C proportion (TOC %), smoothed with generalized additive models (GAMs). **(D)** The proportional contributions of organic matter sources (POM, lake bottom material (aquatic mosses and algae), and terrestrial vegetation to Lake Kuutsjärvi over the Holocene from the end-member mixing modeling. The pale orange background denotes the regional HTM (from 8 to 4 ka cal BP) and the dashed lines the zonation from the cluster analysis on the OM data.

temperature record from Lake Kuutsjärvi supports this notion, although with a more conspicuous rise to the peak thermal maximum at ca. 6–4 cal ka BP compared to previous records (Fig. 7A; Salonen et al., 2024). On the other hand, $\delta^{18}O_{lw}$ records deviating from the Holocene temperature trend have been reported in a few studies from Fennoscandia (St. Amour et al., 2010; Muschitiello et al., 2013). St. Amour et al. (2010) proposed that wintertime circulation changes and weakened zonal circulation (NAO- dominance) gave rise to low $\delta^{18}O_{lw}$ values around 6.5 cal ka BP in Lakes Svartkälstjärn and Spåime in central Sweden. Muschitiello et al. (2013) explained short-term negative excursions during late Holocene in $\delta^{18}O_{lw}$ of Lake Bjärsträsk on Gotland Island, Sweden, as outbreaks of wintertime cold Siberian and the Polar air masses, which led to snow-rich winters replenishing the local aquifer feeding the lake with water depleted in ^{18}O and ^{2}H. The short-term mid-Holocene negative excursion in $\delta^{18}O_{lw}$ in Lake Kuutsjärvi could be explained by a similar mechanism, where prevailing negative winter-time NAO and Siberian High promoted longer winters and snowpack accumulation leading to spring melt and groundwater inputs depleted in ^{18}O. The yellow diatom-rich laminations and more aquatic OM source at ca. 6 cal ka BP appear simultaneous with the low $\delta^{18}O_{lw}$ values at 6.5 cal ka BP. The differences in the temporal resolution, the GAMs and the averaging methods used with each dataset hamper pinpointing a clear temporal correspondence. Nevertheless, a strong wintertime Siberian High with snow-rich winters and higher groundwater levels compared to the HTM average could have led to isotopically light, nutrient-rich groundwater seepage to Lake Kuutsjärvi at around 6.5 cal ka BP, supporting aquatic (diatom) production seen in the lithostratigraphy. Lake nutrient balance, in particular phosphorus and silica inputs in northern oligotrophic closed basins, has been shown to be notably supported by groundwater inflow (e.g. Ala-aho et al., 2013).

The mixing model (Fig. 7C) suggests a predominance of aquatic sources to sediments throughout the Holocene, with a larger contribution of lake bottom vegetation (~25 % of the total OM) to the early Holocene sediments compared to the rest of the sequence, while planktic POM proliferates in the late Holocene (≥50 % of the total sediment OM). The newly formed early Holocene Kuutsjärvi, with a poorly developed catchment, was probably fast colonized by aquatic mosses, often rapidly spreading to newly established postglacial habitats (Väliranta et al., 2015). Allochthonous OM inputs from the soils covered by sparse mountain-birch forest (Shala et al., 2014; Helmens et al., 2018; Salonen et al., 2024) were likely not significant. In contrast, the late Holocene land cover in the region was characterized by northern boreal pine (*Pinus sylvestris*) and spruce (*Picea abies*) forest (Shala et al., 2014; Salonen et al., 2024) and well-developed soils. At this time, Lake Kuutsjärvi probably became a close approximation of the modern lake with increased hydrological connectivity, higher water levels and rapid turnover, flushing OM out of the lake. The late Holocene is also characterized by the lowest $\delta^{18}O_{lw}$ values in the record, which is in line with the cooling temperatures and higher effective humidity. Higher lake water levels and hydrological connectivity are supported by the recovery of profundal chironomid taxa, *Sergentia coracina*-type, and a dominance of *Micropsectra contracta* -type and *Tanytarsus lugens* -type also typical for streams, in the latest stage of the Holocene (Fig. S5). The sediment TOC% indicates overall lower production in the late Holocene, while most of the C appears to be sourced from pelagic sources. A similar shift to planktic algal communities supported by more turbulent lake water column of the wetter and colder late Holocene have been reported based on diatom and pigment analyses from northern Fennoscandia (Reuss et al., 2010; Rantala et al., 2015; Belle et al., 2019). Furthermore, higher lake level enlarged the area for planktic production, and hydrological opening may have eased the drainage of terrestrial material. In addition, the relative rise in $\delta^{15}N$ (Fig. 6) indicates higher nitrogen utilization and aquatic productivity with respect to available N (Wu et al., 2006).

Overall, our results highlight the key role of hydrological connectivity on the sediment C sink: dry periods promoted the C sink and burial of allochtonous C, while wet periods supported C throughflow. Thus, while C burial in northern lakes has shown to have increased (Heathcote et al., 2015), lakes in the future wetter high-latitude Europe may have an increasing role as processors of allochtonous C transported across the land-aquatic gradients.

4. Conclusions

We reconstructed Holocene changes in Lake Kuutsjärvi C burial and OM sourcing together with hydroclimate change in northern Fennoscandia, using elemental (C, N) and stable isotope ($\delta^{13}C$, $\delta^{15}N$, $\delta^{18}O$) records from sediment organic matter and chironomid head capsule chitin. The modern water isotope monitoring indicated that groundwater and snowmelt have a marked impact on the oxygen isotope composition ($\delta^{18}O_{lw}$) of Kuutsjärvi water in early summer during the chironomid larval activity. The reconstructed lake water oxygen isotope composition ($\delta^{18}O_{lw}$) follows the Holocene summer temperature evolution with lower average values in the early Holocene, generally higher values during the HTM, and lower values following the cooling temperatures of the late Holocene. However, a marked negative excursion in $\delta^{18}O_{lw}$ around 6.5 cal ka BP within the warm mid-Holocene suggests wintertime atmospheric circulation changes that led to longer winters and snowpack accumulation, increasing the impact of isotopically depleted spring melt and groundwater on $\delta^{18}O_{lw}$. The Holocene C accumulation rates followed the changes in hydroclimate, vegetation development and sediment accumulation, with an early Holocene increase, the highest CAR at the HTM when the lake level was likely lower, and a clear slowdown at ca. 4 cal ka BP related to basin infilling. Within the HTM, there are two CAR minimums at ca. 8 and 6 cal ka BP linked to yellow, diatom-rich sediment layers with lower TOC% content, indicating high aquatic productivity and nutrient inputs possibly related to the change in wintertime climate and groundwater influence. According to our data and the results from end-member mixing modeling, Lake Kuutsjärvi was dominated by aquatic OM sources throughout the Holocene, with aquatic mosses and benthic algae having more impact in the early Holocene and planktic algae in the late Holocene. In the mid-Holocene, the warm temperatures and longer water residence time, coupled with well-developed soils and Holocene maximum forest density, increased sedimentation of both aquatic and land-derived material. In contrast, land-derived OM contributes less to the burial in the late Holocene despite a likely increase lake level and hydrological connectivity. Our results demonstrate the key role of hydrological connectivity in controlling both burial and sourcing of C, and highlight the need to better identify the different source contributions to high-latitude lake C burial.

CRediT authorship contribution statement

Lilia E. Orozco: Investigation, Methodology, Visualization, Writing – original draft. **Jan Weckström:** Resources, Supervision, Writing – review & editing. **Mateusz Plociennik:** Investigation, Writing – review & editing. **Annika K. Åberg:** Investigation, Methodology, Writing – review & editing. **J. Sakari Salonen:** Resources, Writing – review & editing. **Darren R. Gröcke:** Resources, Writing – review & editing. **Laura Arppe:** Resources, Methodology, Supervision, Writing – review & editing. **Maija Heikkilä:** Conceptualization, Methodology, Resources, Supervision, Funding acquisition, Project administration, Writing – review & editing.

Declaration of competing interest

The authors declare the following financial interests/personal relationships which may be considered as potential competing interests: Maija Heikkila reports financial support was provided by Research Council of Finland. If there are other authors, they declare that they have no known competing financial interests or personal relationships that could have appeared to influence the work reported in this paper.

Acknowledgements

This study was funded by the Research Council of Finland (grant number 334509) and the Finnish Cultural Foundation funding to M.H. J. S.S. received funding from the Research Council of Finland (grant number 331426). We thank the University of Helsinki Värriö Subarctic Research Station for their valuable help with isotope hydrological monitoring and Antti Ojala for making possible the sediment coring. Meeri Näppilä, Sanna Korkonen, Violeta Berlajolli and Antti Jokelainen are thanked for help with sample collection and preparation, and Malin Kylander and Karin Helmens for the valuable comments and discussion that improved the manuscript.

Appendix A. Supplementary data

Supplementary data to this article can be found online at https://doi.org/10.1016/j.quascirev.2025.109323.

Data availability

A link to the data and/or code is provided as part of this submission.

References

Ala-aho, P., Rossi, P.M., Kløve, B., 2013. Interaction of esker groundwater with headwater lakes and streams. J. Hydrol. 500, 144–156. https://doi.org/10.1016/j.jhydrol.2013.07.014.

Andersen, T., Cranston, P.S., Epler, J.H., 2013. Chironomidae of the Holarctic Region: Keys and Diagnoses: Larvae. Scandinavian Society of Entomology.

Anderson, N.J., D'andrea, W., Fritz, S.C., 2009. Holocene carbon burial by lakes in SW Greenland. Glob. Change Biol. 15, 2590–2598.

Anderson, N.J., Heathcote, A.J., Engstrom, D.R., GLOBOCARB DATA Contributors, 2020. Anthropogenic alteration of nutrient supply increases the global freshwater carbon sink. Sci. Adv. 6, eaaw2145. https://doi.org/10.1126/sciadv.aaw2145.

Arppe, L., Kurki, E., Wooller, M.J., Luoto, T.P., Zajączkowski, M., Ojala, A.E., 2017. A 5500-year oxygen isotope record of high arctic environmental change from southern Spitsbergen. Holocene 27, 1948–1962.

Ayala-Borda, P., Lovejoy, C., Power, M., Rautio, M., 2021. Evidence of eutrophication in Arctic lakes. Arct. Sci. 7, 859–871. https://doi.org/10.1139/AS-2020-0033.

Bailey, H., Hubbard, A., Klein, E.S., Mustonen, K.-R., Akers, P.D., Marttila, H., Welker, J. M., 2021. Arctic sea-ice loss fuels extreme European snowfall. Nat. Geosci. 14, 283–288. https://doi.org/10.1038/s41561-021-00719-y.

Bain, J.T., Proctor, M.C.F., 1980. The requirement of aquatic bryophytes for free CO2 as an inorganic carbon source, some experimental evidence. New Phytol. 86, 393–400.

Balascio, N.L., Anderson, R.S., D'Andrea, W.J., Wickler, S., D'Andrea, R.M., Bakke, J., 2020. Vegetation changes and plant wax biomarkers from an ombrotrophic bog define hydroclimate trends and human-environment interactions during the Holocene in northern Norway. Holocene 30, 1849–1865. https://doi.org/10.1177/0959683620950456.

Belle, S., Nilsson, J.L., Tõnno, I., Freiberg, R., Vrede, T., Goedkoop, W., 2019. Climate-induced changes in carbon flows across the plant-consumer interface in a small subarctic lake. Sci. Rep. 9, 17087. https://doi.org/10.1038/s41598-019-53541-3.

Bennett, K., Buck, C.E., 2016. Interpretation of lake sediment accumulation rates. Holocene 26, 1092–1102. https://doi.org/10.1177/0959683616632880.

Blanchet, C.C., Arzel, C., Davranche, A., Kahilainen, K.K., Secondi, J., Taipale, S., Lindberg, H., Loehr, J., Manninen-Johansen, S., Sundell, J., Maanan, M., Nummi, P., 2022. Ecology and extent of freshwater browning - what we know and what should be studied next in the context of global change. Sci. Total Environ. 812, 152420. https://doi.org/10.1016/j.scitotenv.2021.152420.

Bogren, F., 2019. Evidence for Birch Forests and a Highly Productive Environment Near the Margin of the Fennoscandian Ice Sheet in the Värriötunturit Area, Northeastern Finland (M. Sc. Thesis). Department of Physical Geography, University of Stockholm, Stockholm.

Bowen, G.J., Cai, Z., Fiorella, R.P., Putman, A.L., 2019. Isotopes in the water cycle: regional- to global-scale patterns and applications. Annu. Rev. Earth Planet Sci. 47, 453–479. https://doi.org/10.1146/annurev-earth-053018-060220.

Brodie, C.R., Leng, M.J., Casford, J.S.L., Kendrick, C.P., Lloyd, J.M., Yongqiang, Z., Bird, M.I., 2011a. Evidence for bias in C and N concentrations and $\delta^{13}C$ composition of terrestrial and aquatic organic materials due to pre-analysis acid preparation methods. Chem. Geol. 282, 67–83. https://doi.org/10.1016/j.chemgeo.2011.01.007.

Brodie, C.R., Heaton, T.H.E., Leng, M.J., Kendrick, C.P., Casford, J.S.L., Lloyd, J.M., 2011b. Evidence for bias in measured δ^{15}N values of terrestrial and aquatic organic materials due to pre-analysis acid treatment methods. Rapid Commun. Mass Spectrom. 25, 1089–1099. https://doi.org/10.1002/rcm.4970.

Brooks, S.J., Langdon, P.G., Heiri, O., 2007. The identification and use of Palaearctic Chironomidae larvae in palaeoecology. Quat. Res. Assoc. Tech. Guide 1, i–vi.

Burpee, B.T., Saros, J.E., 2020. Cross-ecosystem nutrient subsidies in Arctic and alpine lakes: implications of global change for remote lakes. Environ. Sci. : Process. Impacts 22, 1166–1189.

Butler, M.G., Braegelman, S.D., 2018. Pre-emergence growth and development in the arctic midge Trichotanypus alaskensis Brundin. J. Limnol. 77.

Butterbach-Bahl, K., Gundersen, P., Ambus, P., Augustin, J., Beier, C., Boeckx, P., Dannenmann, M., Sanchez Gimeno, B., Ibrom, A., Kiese, R., Kitzler, B., Rees, R.M., Smith, K.A., Stevens, C., Vesala, T., Zechmeister-Boltenstern, S., 2011. Nitrogen processes in terrestrial ecosystems. In: The European Nitrogen Assessment : Sources, Effects and Policy Perspectives. Cambridge University Press, pp. 99–125. https://doi.org/10.1017/CBO9780511976988.009.

Casas-Ruiz, J.P., Bodmer, P., Bona, K.A., Butman, D., Couturier, M., Emilson, E.J.S., Finlay, K., Genet, H., Hayes, D., Karlsson, J., Paré, D., Peng, C., Striegl, R., Webb, J., Wei, X., Ziegler, S.E., del Giorgio, P.A., 2023. Integrating terrestrial and aquatic ecosystems to constrain estimates of land-atmosphere carbon exchange. Nat. Commun. 14, 1571. https://doi.org/10.1038/s41467-023-37232-2.

Chang, J.C., Shulmeister, J., Gröcke, D.R., Woodward, C.A., 2018. Toward more accurate temperature reconstructions based on oxygen isotopes of subfossil chironomid head-capsules in Australia. Limnol. Oceanogr. 63, 295–307. https://doi.org/10.1002/lno.10630.

Cole, J.J., Prairie, Y.T., Caraco, N.F., McDowell, W.H., Tranvik, L.J., Striegl, R.G., Duarte, C.M., Kortelainen, P., Downing, J.A., Middelburg, J.J., 2007. Plumbing the global carbon cycle: integrating inland waters into the terrestrial carbon budget. Ecosystems 10, 172–185.

Corcoran, M.C., Thomas, E.K., Morrill, C., 2021. Using a paired chironomid δ18O and aquatic leaf wax δ^2H approach to reconstruct seasonality on western Greenland during the Holocene. Paleoceanogr. Paleoclimatol. 36, e2020PA004169.

Danks, H.V., 1971. Overwintering of some north temperate and arctic chironomidae: ii. Chironomid biology. Can. Entomol. 103, 1875–1910. https://doi.org/10.4039/Ent1031875-12.

Danks, H.V., Oliver, D.R., 1972. Seasonal emergence of some high arctic chironomidae (diptera). Can. Entomol. 104, 661–686. https://doi.org/10.4039/Ent104661-5.

Dansgaard, W., 1964. Stable isotopes in precipitation. Tellus 16, 436–468. https://doi.org/10.1111/j.2153-3490.1964.tb00181.x.

Dombrosky, J., 2020. A ~1000-year ^{13}C Suess correction model for the study of past ecosystems. Holocene 30, 474–478. https://doi.org/10.1177/0959683619887416.

Downing, J.A., Prairie, Y.T., Cole, J.J., Duarte, C.M., Tranvik, L.J., Striegl, R.G., McDowell, W.H., Kortelainen, P., Caraco, N.F., Melack, J.M., 2006. The global abundance and size distribution of lakes, ponds, and impoundments. Limnol. Oceanogr. 51, 2388–2397.

England, M.R., Eisenman, I., Lutsko, N.J., Wagner, T.J.W., 2021. The recent emergence of arctic amplification. Geophys. Res. Lett. 48, e2021GL094086. https://doi.org/10.1029/2021GL094086.

Ferland, M.-E., del Giorgio, P.A., Teodoru, C.R., Prairie, Y.T., 2012. Long-term C accumulation and total C stocks in boreal lakes in northern Québec. Glob. Biogeochem. Cycles 26, GB0E04. https://doi.org/10.1029/2011GB004241.

Finlay, J.C., Kendall, C., 2007. Stable isotope tracing of temporal and spatial variability in organic matter sources to freshwater ecosystems. In: Stable Isotopes in Ecology and Environmental Science. John Wiley & Sons, Ltd, pp. 283–333. https://doi.org/10.1002/9780470691854.ch10.

Finnish Meteorological Institute, 2022. Finnish Meteorological Institute. https://en.ilmatieteenlaitos.fi/statistics-from-1961-onwards (accessed 9.7.22).

France, R.L., 1995. Differentiation between littoral and pelagic food webs in lakes using stable carbon isotopes. Limnol. Oceanogr. 40, 1310–1313. https://doi.org/10.4319/lo.1995.40.7.1310.

Gat, J.R., 1996. Oxygen and hydrogen isotopes in the hydrologic cycle. Annu. Rev. Earth Planet Sci. 24, 225–262. https://doi.org/10.1146/annurev.earth.24.1.225.

Govan, E., Parnell, A., 2023. Simmr: A Stable Isotope Mixing Model.

Gröning, M., Lutz, H.O., Roller-Lutz, Z., Kralik, M., Gourcy, L., Pöltenstein, L., 2012. A simple rain collector preventing water re-evaporation dedicated for δ^{18}O and δ^2H analysis of cumulative precipitation samples. J. Hydrol. 448, 195–200.

Hammarlund, D., Björck, S., Buchardt, B., Israelson, C., Thomsen, C.T., 2003. Rapid hydrological changes during the Holocene revealed by stable isotope records of lacustrine carbonates from Lake Igelsjön, southern Sweden. Quat. Sci. Rev. 22, 353–370. https://doi.org/10.1016/S0277-3791(02)00091-4.

Hanson, P.C., Pace, M.L., Carpenter, S.R., Cole, J.J., Stanley, E.H., 2015. Integrating landscape carbon cycling: research needs for resolving organic carbon budgets of lakes. Ecosystems 18, 363–375. https://doi.org/10.1007/s10021-014-9826-9.

Heathcote, A., Anderson, N., Prairie, Y., Engstrom, D.R., del Giorgio, P.A., 2015. Large increases in carbon burial in northern lakes during the Anthropocene. Nat. Commun. 6, 10016. https://doi.org/10.1038/ncomms10016.

Heikkilä, M., Edwards, T.W.D., Seppä, H., Sonninen, E., 2010. Sediment isotope tracers from Lake Saarikko, Finland, and implications for Holocene hydroclimatology. Quat. Sci. Rev. 29, 2146–2160. https://doi.org/10.1016/j.quascirev.2010.05.010.

Heiri, O., Lotter, A.F., Lemcke, G., 2001. Loss on ignition as a method for estimating organic and carbonate content in sediments: reproducibility and comparability of results. J. Paleolimnol. 25, 101–110. https://doi.org/10.1023/A:1008119611481.

Helmens, K.F., Katrantsiotis, C., Salonen, J.S., Shala, S., Bos, J.A., Engels, S., Kuosmanen, N., Luoto, T.P., Väliranta, M., Luoto, M., 2018. Warm summers and rich biotic communities during N-Hemisphere deglaciation. Global Planet. Change 167, 61–73.

Hyvärinen, H., Alhonen, P., 1994. Holocene lake-level changes in the Fennoscandian tree-line region, western Finnish Lapland: diatom and cladoceran evidence. Holocene 4, 251–258. https://doi.org/10.1177/095968369400400304.

Johansson, P., 1995. The deglaciation in the eastern part of the weichselian ice divide in Finnish lapland: with 42 figures and one appended map. Geol. Tutkimusk.

Johnston, S.E., Striegl, R.G., Bogard, M.J., Dornblaser, M.M., Butman, D.E., Kellerman, A.M., Wickland, K.P., Podgorski, D.C., Spencer, R.G.M., 2020. Hydrologic connectivity determines dissolved organic matter biogeochemistry in northern high-latitude lakes. Limnol. Oceanogr. 65, 1764–1780. https://doi.org/10.1002/lno.11417.

Jonsson, C.E., Andersson, S., Rosqvist, G.C., Leng, M.J., 2010. Reconstructing past atmospheric circulation changes using oxygen isotopes in lake sediments from Sweden. Clim. Past 6, 49–62. https://doi.org/10.5194/cp-6-49-2010.

Juggins, S., 2019. Package 'rioja.' RCRAN.

Karlsson, J., Byström, P., Ask, J., Ask, P., Persson, L., Jansson, M., 2009. Light limitation of nutrient-poor lake ecosystems. Nature 460, 506–509. https://doi.org/10.1038/nature08179.

Kjellman, S.E., Thomas, E.K., Schomacker, A., 2022. Arctic and sub-Arctic lake water δ^2H and δ^{18}O along a coastal-inland transect: implications for interpreting water isotope proxy records. J. Hydrol. 607, 127556. https://doi.org/10.1016/j.jhydrol.2022.127556.

Korhola, A., Tikkanen, M., Weckström, J., 2005. Quantification of Holocene lake-level changes in Finnish Lapland using a cladocera – lake depth transfer model. J. Paleolimnol. 34, 175–190. https://doi.org/10.1007/s10933-005-1839-0.

Kortelainen, P., Pajunen, H., Rantakari, M., Saarnisto, M., 2004. A large carbon pool and small sink in boreal Holocene lake sediments. Glob. Change Biol. 10, 1648–1653.

Krikunova, A.I., Kostromina, N.A., Savelieva, L.A., Tolstobrov, D.S., Petrov, A.Y., Long, T., Kobe, F., Leipe, C., Tarasov, P.E., 2022. Late- and postglacial vegetation and climate history of the central Kola Peninsula derived from a radiocarbon-dated pollen record of Lake Kamenistoe. Palaeogeogr. Palaeoclimatol. Palaeoecol. 603, 111191. https://doi.org/10.1016/j.palaeo.2022.111191.

Kuhn, C., Butman, D., 2021. Declining greenness in Arctic-boreal lakes. Proc. Natl. Acad. Sci. USA 118, e2021219118. https://doi.org/10.1073/pnas.2021219118.

Lackmann, A.R., Butler, M.G., 2018. Breaking the rule: five larval instars in the podonomine midge Trichotanypus alaskensis Brundin from Barrow, Alaska. J. Limnol. 77.

Lamb, A.L., Wilson, G.P., Leng, M.J., 2006. A review of coastal palaeoclimate and relative sea-level reconstructions using δ^{13}C and C/N ratios in organic material. Earth Sci. Rev. 75, 29–57.

Lamb, A.L., Barst, B.D., Elder, C.D., Engels, S., Francis, C., van Hardenbroek, M., Heiri, O., Lombino, A., Robson, H.J., Walter Anthony, K., Wooller, M.J., 2024. Stable isotope analyses of lacustrine chitinous invertebrate remains: analytical advances, challenges and potential. Quat. Sci. Rev. 346, 109067. https://doi.org/10.1016/j.quascirev.2024.109067.

Lasher, G.E., Axford, Y., McFarlin, J.M., Kelly, M.A., Osterberg, E.C., Berkelhammer, M. B., 2017. Holocene temperatures and isotopes of precipitation in Northwest Greenland recorded in lacustrine organic materials. Quat. Sci. Rev. 170, 45–55. https://doi.org/10.1016/j.quascirev.2017.06.016.

Lenz, M., Savelieva, L., Frolova, L., Cherezova, A., Moros, M., Baumer, M.M., Gromig, R., Kostromina, N., Nigmatullin, N., Kolka, V., Wagner, B., Fedorov, G., Melles, M., 2021. Lateglacial and Holocene environmental history of the central Kola region, northwestern Russia revealed by a sediment succession from Lake Imandra. Boreas 50, 76–100. https://doi.org/10.1111/bor.12465.

Lombino, A., Atkinson, T., Brooks, S.J., Gröcke, D.R., Holmes, J., Jones, V.J., Marshall, J. D., 2021. Experimental determination of the temperature dependence of oxygen-isotope fractionation between water and chitinous head capsules of chironomid larvae. J. Paleolimnol. 66, 117–124. https://doi.org/10.1007/s10933-021-00191-z.

Mäkisara, K., Katila, M., Peräsaari, J., 2019. The multi-source national forest inventory of Finland – methods and results 2015. Luonnonvarakeskus.

Marttila, H., Lohila, A., Ala-Aho, P., Noor, K., Welker, J.M., Croghan, D., Mustonen, K., Meriö, L.-J., Autio, A., Muhic, F., Bailey, H., Aurela, M., Vuorenmaa, J., Penttilä, T., Hyöky, V., Klein, E., Kuzmin, A., Korpelainen, P., Kumpula, T., Rauhala, A., Kløve, B., 2021. Subarctic catchment water storage and carbon cycling – leading the way for future studies using integrated datasets at Pallas. Finland. Hydrol. Process. 35, e14350. https://doi.org/10.1002/hyp.14350.

Mauri, A., Davis, B.A.S., Collins, P.M., Kaplan, J.O., 2015. The climate of Europe during the Holocene: a gridded pollen-based reconstruction and its multi-proxy evaluation. Quat. Sci. Rev. 112, 109–127. https://doi.org/10.1016/j.quascirev.2015.01.013.

Mayewski, P.A., Rohling, E.E., Stager, J.C., Karlén, W., Maasch, K.A., Meeker, L.D., Meyerson, E.A., Gasse, F., Kreveld, S. van, Holmgren, K., Lee-Thorp, J., Rosqvist, G., Rack, F., Staubwasser, M., Schneider, R.R., Steig, E.J., 2004. Holocene climate variability. Quat. Res. 62, 243–255. https://doi.org/10.1016/j.yqres.2004.07.001.

McCrystall, M.R., Stroeve, J., Serreze, M., Forbes, B.C., Screen, J.A., 2021. New climate models reveal faster and larger increases in Arctic precipitation than previously projected. Nat. Commun. 12, 6765. https://doi.org/10.1038/s41467-021-27031-y.

McGowan, S., Anderson, N.J., Edwards, M.E., Hopla, E., Jones, V., Langdon, P.G., Law, A., Solovieva, N., Turner, S., van Hardenbroek, M., Whiteford, E.J., Wiik, E., 2018. Vegetation transitions drive the autotrophy–heterotrophy balance in Arctic lakes. Limnol. Oceanogr. Lett. 3, 246–255. https://doi.org/10.1002/lol2.10086.

Meyers, P.A., 2003. Applications of organic geochemistry to paleolimnological reconstructions: a summary of examples from the Laurentian Great Lakes. Org. Geochem. 34, 261–289.

Milardi, M., Petäjä, T., Weckström, J., 2019. Should we further investigate the cascading effects of introduced fish on insectivorous birds? Boreal Environ. Res. 24, 51–62.

Moller Pillot, H.K.M., 2009. Chironomidae larvae. In: Chironomini: Biology and Ecology of the Chironomini, vol. 2. BRILL.
Moller Pillot, H.K.M., 2014. Chironomidae larvae. In: Orthocladiinae: Biology and Ecology of the Aquatic Orthocladiinae, vol. 3. Hotei Publishing.
Muschitiello, F., Schwark, L., Wohlfarth, B., Sturm, C., Hammarlund, D., 2013. New evidence of Holocene atmospheric circulation dynamics based on lake sediments from southern Sweden: a link to the Siberian High. Quat. Sci. Rev. 77, 113–124. https://doi.org/10.1016/j.quascirev.2013.07.026.
National Land Survey of Finland, 2014. Elevation Model 2 M.
Neal, A., 2004. Ground-penetrating radar and its use in sedimentology: principles, problems and progress. Earth Sci. Rev. 66, 261–330. https://doi.org/10.1016/j.earscirev.2004.01.004.
Oliver, D.R., 1968. Adaptations of arctic chironomidae. Ann. Zool. Fenn. 5, 111–118.
Osburn, C.L., Anderson, N.J., Leng, M.J., Barry, C.D., Whiteford, E.J., 2019. Stable isotopes reveal independent carbon pools across an Arctic hydro-climatic gradient: implications for the fate of carbon in warmer and drier conditions. Limnol. Oceanogr. Lett. 4, 205–213.
Otiniano, G.A., Porter, T.J., Phillips, M.A., Juutinen, S., Weckström, J.B., Heikkilä, M.P., 2024. Reconstructing warm-season temperatures using brGDGTs and assessing biases in Holocene temperature records in northern Fennoscandia. Quat. Sci. Rev. 329, 108555. https://doi.org/10.1016/j.quascirev.2024.108555.
Pajunen, H., 2000. Carbon in Finnish lake sediments. Special Paper 29. Geological Survey of Finland, Espoo, Finland, p. 92.
Parnell, A.C., Inger, R., Bearhop, S., Jackson, A.L., 2010. Source partitioning using stable isotopes: coping with too much variation. PLoS One 5, e9672.
Pfalz, G., Diekmann, B., Freytag, J.-C., Biskaborn, B.K., 2023. Effect of temperature on carbon accumulation in northern lake systems over the past 21,000 years. Front. Earth Sci. 11. https://doi.org/10.3389/feart.2023.1233713.
Putkinen, S., Saarelainen, J., 1998. Kullenbergin näytteenottimen uusi kevennetty malli. Geologi 50, 2.
R Core Team, 2023. R: A Language and Environment for Statistical Computing.
Rantala, M., Luoto, T., Nevalainen, L., 2015. Temperature controls organic carbon sequestration in a subarctic lake. Sci. Rep. 6, 34780. https://doi.org/10.1038/srep34780.
Rawlins, M.A., Steele, M., Holland, M.M., Adam, J.C., Cherry, J.E., Francis, J.A., Rantala, M.V., Luoto, T.P., Weckström, J., Perga, M.-E., Rautio, M., Nevalainen, L., 2015. Climate controls on the Holocene development of a subarctic lake in northern Fennoscandia. Quat. Sci. Rev. 126, 175–185. https://doi.org/10.1016/j.quascirev.2015.08.032.
Renberg, I., Hansson, H., 2008. The HTH sediment corer. J. Paleolimnol. 40, 655–659. https://doi.org/10.1007/s10933-007-9188-9.
Renssen, H., Seppä, H., Crosta, X., Goosse, H., Roche, D.M., 2012. Global characterization of the Holocene thermal maximum. Quat. Sci. Rev. 48, 7–19. https://doi.org/10.1016/j.quascirev.2012.05.022.
Reuss, N., Leavitt, P.R., Hall, R.I., Bigler, C., Hammarlund, D., 2010. Development and application of sedimentary pigments for assessing effects of climatic and environmental changes on subarctic lakes in northern Sweden. J. Paleolimnol. 43, 149–169. https://doi.org/10.1007/s10933-009-9323-x.
Riis, T., Sand-Jensen, K., 1997. Growth reconstruction and photosynthesis of aquatic mosses: influence of light, temperature and carbon dioxide at depth. J. Ecol. 85, 359–372. https://doi.org/10.2307/2960508.
Riis, T., Christoffersen, K.S., Baattrup-Pedersen, A., 2016. Mosses in High-Arctic lakes: in situ measurements of annual primary production and decomposition. Polar Biol. 39, 543–552. https://doi.org/10.1007/s00300-015-1806-9.
Rozanski, K., Araguás-Araguás, L., Gonfiantini, R., 1993. Isotopic patterns in modern global precipitation. In: Climate Change in Continental Isotopic Records. American Geophysical Union (AGU), pp. 1–36. https://doi.org/10.1029/GM078p0001.
Ruosteenoja, K., Markkanen, T., Räisänen, J., 2020. Thermal seasons in northern Europe in projected future climate. Int. J. Climatol. 40, 4444–4462. https://doi.org/10.1002/joc.6466.
Sachse, D., Billault, I., Bowen, G.J., Chikaraishi, Y., Dawson, T.E., Feakins, S.J., Freeman, K.H., Magill, C.R., McInerney, F.A., Van Der Meer, M.T., Polissar, P., Robins, R.J., Sachs, J.P., Schmidt, H.-L., Sessions, A.L., White, J.W.C., West, J.B., Kahmen, A., 2012. Molecular paleohydrology: interpreting the hydrogen-isotopic composition of lipid biomarkers from photosynthesizing organisms. Annu. Rev. Earth Planet Sci. 40, 221–249. https://doi.org/10.1146/annurev-earth-042711-105535.
Salonen, J.S., Kuosmanen, N., Alsos, I.G., Heintzman, P.D., Rijal, D.P., Schenk, F., Bogren, F., Luoto, M., Philip, A., Piilo, S., Trasune, L., Väliranta, M., Helmens, K.F., 2024. Uncovering Holocene climate fluctuations and ancient conifer populations: insights from a high-resolution multi-proxy record from Northern Finland. Global Planet. Change 237, 104462. https://doi.org/10.1016/j.gloplacha.2024.104462.
Saros, J.E., Arp, C.D., Bouchard, F., Comte, J., Couture, R.-M., Dean, J.F., Lafrenière, M., MacIntyre, S., McGowan, S., Rautio, M., Prater, C., Tank, S.E., Walvoord, M., Wickland, K.P., Antoniades, D., Ayala-Borda, P., Canario, J., Drake, T.W., Folhas, D., Hazuková, V., Kivilä, H., Klanten, Y., Lamoureux, S., Laurion, I., Pilla, R.M., Vonk, J. E., Zolkos, S., Vincent, W.F., 2023. Sentinel responses of Arctic freshwater systems to climate: linkages, evidence, and a roadmap for future research. Arct. Sci. 9, 356–392. https://doi.org/10.1139/as-2022-0021.
Schulze, E., 1994. A key to the larval chironomidae and their instars from Austrian danube region streams and rivers with particular reference to a numerical taxonomic approach. Part I. In: Wasser und Abwasser, Supplementband 3/93. Hrsg.: Bundesamt für Wassergüte, Wien-Kaisermühlen. Schriftenleitung: Werner Kohl. Selbstverlag, 1993, 514 S., öS 562,, vol. 22. Acta hydrochimica et hydrobiologica. https://doi.org/10.1002/aheh.19940220411, 191–191.
Sejrup, H.P., Seppä, H., McKay, N.P., Kaufman, D.S., Geirsdóttir, Á., de Vernal, A., Renssen, H., Husum, K., Jennings, A., Andrews, J.T., 2016. North Atlantic-Fennoscandian Holocene climate trends and mechanisms. Quaternary Science Reviews, Special Issue: PAST Gateways (Palaeo-Arctic Spatial and Temporal Gateways) 147, 365–378. https://doi.org/10.1016/j.quascirev.2016.06.005.
Seppä, H., Birks, H.J.B., 2001. Mean temperature and annual precipitation trends during the Holocene in the Fennoscandian tree-line area: pollen-based climate reconstructions. Holocene 11, 527–539.
Seppä, H., Hammarlund, D., 2000. Pollen-stratigraphical evidence of Holocene hydrological change in northern Fennoscandia supported by independent isotopic data. J. Paleolimnol. 24, 69–79. https://doi.org/10.1023/A:1008169800682.
Seppä, H., MacDonald, G.M., Birks, H.J.B., Gervais, B.R., Snyder, J.A., 2008. Late-Quaternary summer temperature changes in the northern-European tree-line region. Quat. Res. 69, 404–412. https://doi.org/10.1016/j.yqres.2008.02.002.
Seppä, H., Bjune, A.E., Telford, R.J., Birks, H.J.B., Veski, S., 2009. Last nine-thousand years of temperature variability in Northern Europe. Clim. Past 5, 523–535. https://doi.org/10.5194/cp-5-523-2009.
Shala, S., Helmens, K.F., Jansson, K.N., Kylander, M.E., Risberg, J., Löwemark, L., 2014. Palaeoenvironmental record of glacial lake evolution during the early Holocene at Sokli, NE Finland. Boreas 43, 362–376.
Shala, S., Helmens, K.F., Luoto, T.P., Salonen, J.S., Väliranta, M., Weckström, J., 2017. Comparison of quantitative Holocene temperature reconstructions using multiple proxies from a northern boreal lake. Holocene 27, 1745–1755. https://doi.org/10.1177/0959683617708442.
Siitonen, S., Väliranta, M., Weckström, J., Juutinen, S., Korhola, A., 2011. Comparison of Cladocera-based water-depth reconstruction against other types of proxy data in Finnish Lapland. Hydrobiologia 676, 155–172. https://doi.org/10.1007/s10750-011-0885-z.
Smol, J.P., Wolfe, A.P., Birks, H.J.B., Douglas, M.S.V., Jones, V.J., Korhola, A., Pienitz, R., Rühland, K., Sorvari, S., Antoniades, D., Brooks, S.J., Fallu, M., Hughes, M., Keatley, B.E., Laing, T.E., Michelutti, N., Nazarova, L., Nyman, M., Paterson, A.M., Perren, B., Quinlan, R., Rautio, M., Saulnier-Talbot, É., Siitonen, S., Solovieva, N., Weckström, J., 2005. Climate-driven regime shifts in the biological communities of arctic lakes. Proc. Natl. Acad. Sci. USA 102, 4397–4402. https://doi.org/10.1073/pnas.0500245102.
Soto, D.X., Wassenaar, L.I., Hobson, K.A., 2013. Stable hydrogen and oxygen isotopes in aquatic food webs are tracers of diet and provenance. Funct. Ecol. 27, 535–543.
St. Amour, N.A., Hammarlund, D., Edwards, T.W.d., Wolfe, B.B., 2010. New insights into Holocene atmospheric circulation dynamics in central Scandinavia inferred from oxygen-isotope records of lake-sediment cellulose. Boreas 39, 770–782. https://doi.org/10.1111/j.1502-3885.2010.00169.x.
Stevenson, M.A., McGowan, S., Pearson, E.J., Swann, G.E.A., Leng, M.J., Jones, V.J., Bailey, J.J., Huang, X., Whiteford, E., 2021. Anthropocene climate warming enhances autochthonous carbon cycling in an upland Arctic lake, Disko Island, West Greenland. Biogeosciences 18, 2465–2485. https://doi.org/10.5194/bg-18-2465-2021.
Stroeven, A.P., Hättestrand, C., Kleman, J., Heyman, J., Fabel, D., Fredin, O., Goodfellow, B.W., Harbor, J.M., Jansen, J.D., Olsen, L., 2016. Deglaciation of fennoscandia. Quat. Sci. Rev. 147, 91–121.
Talbot, M.R., 1990. A review of the palaeohydrological interpretation of carbon and oxygen isotopic ratios in primary lacustrine carbonates. Chem. Geol. Isot. Geosci. 80, 261–279. https://doi.org/10.1016/0168-9622(90)90009-2.
Tallberg, P., Opfergelt, S., Cornelis, J.-T., Liljendahl, A., Weckström, J., 2015. High concentrations of amorphous, biogenic Si (BSi) in the sediment of a small high-latitude lake: implications for biogeochemical Si cycling and for the use of BSi as a paleoproxy. Aquat. Sci. 77, 293–305.
Thompson, H.A., White, J.R., Pratt, L.M., 2018. Spatial variation in stable isotopic composition of organic matter of macrophytes and sediments from a small Arctic lake in west Greenland. Arctic Antarct. Alpine Res. 50, S100017.
Trancoso, R., Syktus, J., Allan, R.P., Croke, J., Hoegh-Guldberg, O., Chadwick, R., 2024. Significantly wetter or drier future conditions for one to two thirds of the world's population. Nat. Commun. 15, 483. https://doi.org/10.1038/s41467-023-44513-3.
Tranvik, L.J., Downing, J.A., Cotner, J.B., Loiselle, S.A., Striegl, R.G., Ballatore, T.J., Dillon, P., Finlay, K., Fortino, K., Knoll, L.B., 2009. Lakes and reservoirs as regulators of carbon cycling and climate. Limnol. Oceanogr. 54, 2298–2314.
Väliranta, M., Salonen, J.S., Heikkilä, M., Amon, L., Helmens, K., Klimaschewski, A., Kuhry, P., Kultti, S., Poska, A., Shala, S., Veski, S., Birks, H.H., 2015. Plant macrofossil evidence for an early onset of the Holocene summer thermal maximum in northernmost Europe. Nat. Commun. 6, 6809. https://doi.org/10.1038/ncomms7809.
Vallenduuk, H.J., Moller Pillot, H.K.M., 2007. Chironomidae larvae. In: Tanypodinae: General Ecology and Tanypodinae, vol. 1. BRILL.
van Hardenbroek, M., Chakraborty, A., Davies, K.L., Harding, P., Heiri, O., Henderson, A. C.G., Holmes, J.A., Lasher, G.E., Leng, M.J., Panizzo, V.N., Roberts, L., Schilder, J., Trueman, C.N., Wooller, M.J., 2018. The stable isotope composition of organic and inorganic fossils in lake sediment records: current understanding, challenges, and future directions. Quat. Sci. Rev. 196, 154–176. https://doi.org/10.1016/j.quascirev.2018.08.003.
Verbruggen, F., Heiri, O., Reichart, G.J., Blaga, C., Lotter, A.F., 2011. Stable oxygen isotopes in chironomid and cladoceran remains as indicators for lake-water δ18O. Limnol. Oceanogr. 56, 2071–2079.
Verpoorter, C., Kutser, T., Seekell, D.A., Tranvik, L.J., 2014. A global inventory of lakes based on high-resolution satellite imagery. Geophys. Res. Lett. 41, 6396–6402. https://doi.org/10.1002/2014GL060641.
Walker, I.R., 1987. Chironomidae (Diptera) in paleoecology. Quat. Sci. Rev. 6, 29–40. https://doi.org/10.1016/0277-3791(87)90014-X.

Wang, Y.V., O'brien, D.M., Jenson, J., Francis, D., Wooller, M.J., 2009. The influence of diet and water on the stable oxygen and hydrogen isotope composition of Chironomidae (Diptera) with paleoecological implications. Oecologia 160, 225–233.

Webb, E.E., Liljedahl, A.K., Cordeiro, J.A., Loranty, M.M., Witharana, C., Lichstein, J.W., 2022. Permafrost thaw drives surface water decline across lake-rich regions of the Arctic. Nat. Clim. Change 12, 841–846. https://doi.org/10.1038/s41558-022-01455-w.

Wood, S.N., 2017. Generalized Additive Models: an Introduction with R 2 an Introduction with R. Generalized Additive Models, vol. 10. 9781315370279.

Wooller, M.J., Francis, D., Fogel, M.L., Miller, G.H., Walker, I.R., Wolfe, A.P., 2004. Quantitative paleotemperature estimates from δ 18 O of chironomid head capsules preserved in arctic lake sediments. J. Paleolimnol. 31, 267–274.

Woolway, R.I., Kraemer, B.M., Lenters, J.D., Merchant, C.J., O'Reilly, C.M., Sharma, S., 2020. Global lake responses to climate change. Nat. Rev. Earth Environ. 1, 388–403. https://doi.org/10.1038/s43017-020-0067-5.

Wrona, F.J., Johansson, M., Culp, J.M., Jenkins, A., Mård, J., Myers-Smith, I.H., Prowse, T.D., Vincent, W.F., Wookey, P.A., 2016. Transitions in Arctic ecosystems: ecological implications of a changing hydrological regime. J. Geophys. Res.: Biogeosciences 121, 650–674. https://doi.org/10.1002/2015JG003133.

Wu, J., Lin, L., Gagan, M.K., Schleser, G.H., Wang, S., 2006. Organic matter stable isotope (δ13C, δ15N) response to historical eutrophication of Lake taihu, China. Hydrobiologia 563, 19–29. https://doi.org/10.1007/s10750-005-9133-8.

Zeileis, A., Grothendieck, G., Ryan, J.A., Andrews, F., Zeileis, M.A., 2014. Package 'zoo.' R package version, 1, 7–12.